



**A REVIEW OF AERONAUTICAL FATIGUE AND  
STRUCTURAL INTEGRITY IN ISRAEL**  
(April 2013 – March 2015)



**Compiled by:**  
**Dr. Yuval Freed**  
*Engineering Division*  
*Israel Aerospace Industries*  
*Ben-Gurion Airport, Israel*  
*yfreed@iai.co.il*

**Presented at the 34<sup>th</sup> Conference of the International Committee on  
Aeronautical Fatigue and Structural Integrity (ICAF)**  
**Helsinki, Finland**  
**1-2 June 2013**



# **A REVIEW OF AERONAUTICAL FATIGUE AND STRUCTURAL INTEGRITY IN ISRAEL**

**APRIL 2013 – MARCH 2015**

## **SUMMARY**

This review summarizes fatigue, structural-integrity and fracture-mechanics investigations that were performed in Israel during the period of April 2013 to March 2015. The review includes contributions from Israel Aerospace Industries Ltd. (IAI), Israel Air Force (IAF), Tel-Aviv University (TAU), Ben-Gurion University (BGU), Technion and Rafael.

**Presented at the 34<sup>th</sup> ICAF Conference  
Helsinki, Finland  
1-2 June 2015**



## TABLE OF CONTENTS

	Page
1 INTRODUCTION .....	4
2 FATIGUE ANALYSIS, TESTING AND LIFE EXTENSION .....	5
3 STRUCTURAL INTEGRITY OF COMPOSITE MATERIALS .....	22
4 PROBABILISTIC STUDIES .....	27
5 STRUCTURAL HEALTH MONITORING .....	31
6 MISCELLANEOUS .....	36
7 REFERENCES .....	43



## **A REVIEW OF AERONAUTICAL FATIGUE INVESTIGATIONS IN ISRAEL APRIL 2013 – MARCH 2015**

### **1. INTRODUCTION**

The Israel National Review summarizes activities performed in the field of aeronautical fatigue, structural integrity, health monitoring and fracture mechanics in Israel during the period of April 2013 to March 2015. The previous National Review [1] covered activities up to March 2013. The following organizations contributed to this review:

Israel Aerospace Industries Ltd. (IAI)  
Israel Air Force (IAF)  
Tel-Aviv University (TAU)  
Ben-Gurion University (BGU)  
Technion  
Rafael

The National Review was compiled by Dr. Yuval Freed (yfreed@iai.co.il).

## 2. FATIGUE ANALYSIS, TESTING AND LIFE EXTENSION

### 2.1 Investigation of Crack Nucleation in the Vicinity of Cold-Worked Fastener Holes (Y. Freed, O. Dolev, Y. Amran, IAI)

The cold-working procedure is considered as a cost-effective solution to fatigue cracks in metallic structures, and is widely used in the aerospace industries in the past two decades. The split sleeve cold expansion is accomplished by pulling a mandrel, pre fitted with lubricated split sleeve, through an undersized hole in metallic structure (mainly aluminum, steel and titanium). The removal of the sleeve results in a uniform radial expansion of the hole, creating residual compressive stresses in the vicinity of the fastener holes. These compressive stresses are still significant, even after rimming the fastener hole to its nominal size. The residual compressive stresses effectively "shield" the hole from the cyclic tensile stress loads that cause cracks to form and grow, and improve the fatigue and damage tolerance characteristics of the structure.

As part of a damage-tolerance certification program of one of Israel Aerospace Industries business jets, a structurally complete test-article is currently fatigue tested for two lifetimes (40,000 flights) followed by half a lifetime (10,000 flights) of damage-tolerance testing, with artificial flaws inflicted at critical locations. Residual strength tests, under limit loads and cabin pressurization, will be performed in the presence of large cracks at several critical locations. This will be followed by a selected teardown inspection.

During one of the scheduled inspections conducted within the full scale testing, a single crack was inspected at the side windshield retainer, between the window cutout and the nearby fastener hole. The fastener hole was cold-worked during the aircraft assembly process, to enhance its expected fatigue lifetime. The crack was detected and verified by means of two different NDI methods, namely, High Frequency Eddy Current (HFEC) and detailed visual inspection. The crack upon its first detection is shown in Figure 1. The windshield retainer is considered as principal structural element. However, its failure does not lead to immediate catastrophic failure of the aircraft, since the loads applied on the retainer are redistributed and are taken by the cockpit side post.



**Figure 1. (a) cracked retainer. (b) Zoomed view of the crack between the window cutout and the nearby fastener hole**

As part of a root cause analysis conducted, a detailed finite element model was constructed. The analysis consisted of two stages:

- **Stage I:** Simulation of the cold-working process – The mandrel insertion and removal was simulated by means of StressCheck built-in fastener elements assuming interference of 4% in the hole diameter. Nonlinear analysis was conducted to accurately obtain the residual stresses that are induced after mandrel removal. For simplicity, the cold-working process was applied only to the fastener hole in which the crack was detected in.
- **Stage II:** Simulation of the load application after mandrel removal. The load was determined based on far field strain gauge measurements during application of pressurization cycle in test.

The radial and principal stress distributions after completion of the cold-working procedure and mandrel removal (stage I) is shown in Figure 2a and b, respectively. The significant compressive stresses near the cold-worked

fastener hole as well as the moderate residual far-field tensile stresses are clearly shown in Figure 2a. The interaction between the nearby stress concentration (associated with cutout radius) and the cold-worked hole is depicted in Figure 2b. The corresponding residual tensile stresses were determined as 62.6 MPa (9.1 ksi).

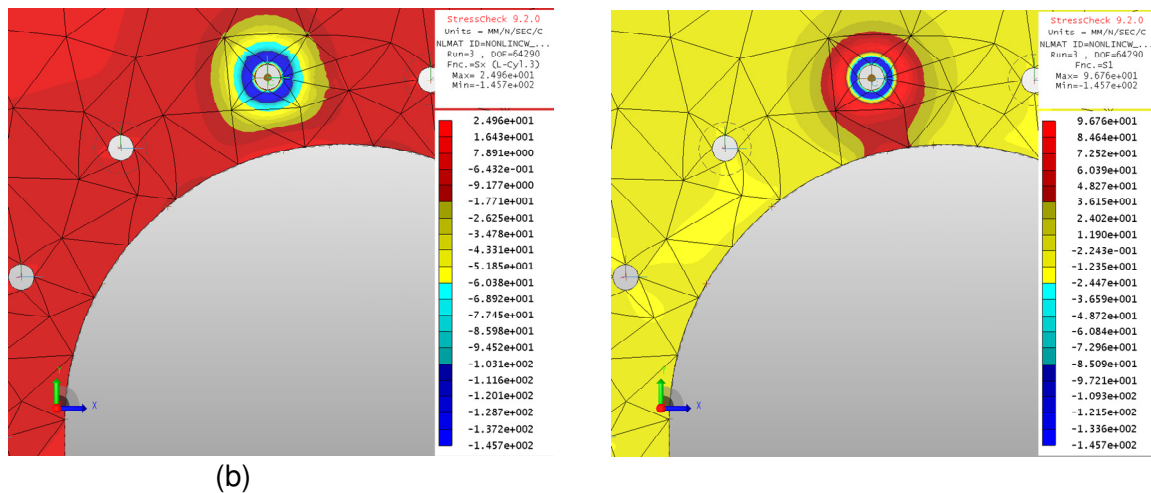


**Figure 2. (a) Radial stress distribution after completion of cold-working process and mandrel removal. (b) Principal stress distribution after completion of cold-working process and mandrel removal.**

After completion of simulating the cold-working procedure, loads that represent the aircraft pressurization cycle were applied in the finite element analysis. The loads were determined based on strain gauge measurements in test. Ramberg-Osgood elasto-plastic model was employed to represent the non-linear behavior of the aluminum. The region in the vicinity of the cutout radius was found to be characterized by high stress level, and yields upon application of pressurization cycle. The peak stress was obtained as 364.3 MPa (52.8 ksi), which is above the yield strength of the aluminum. It may be noted that the peak stress is located at the cutout radius and not at the nearby fastener hole. This implies that the location of crack nucleation is at the cutout radius. Similar conclusions were reported in the past by Brot and Matias [2, 3], in which the effect of residual tensile stresses induced by cold-working to a fastener hole can dramatically reduce the crack nucleation period in a case of a stress concentration.

Based on the FEM results, fatigue analysis was conducted to obtain the crack nucleation period. This was followed by crack growth analysis. The overall lifetime of the windshield retainer was then determined and compared to test findings; descent agreement was reached.

A full length paper describing the root cause analysis, FEM predictions and the corresponding fractographic investigation may be found in Ref. [4].

## 2.2 IAI Executive Jet – Full Scale Fatigue Testing (Y. Freed, IAI)

This activity is a continuation of an activity that was reported in the 2013 Israel National Review [1].

Israel Aerospace Industries and the Gulfstream Aerospace Corporation have jointly developed a new super mid-size executive jet. The aircraft has a range of 3,400 nautical miles at a maximum speed of Mach 0.85. It can cruise at altitudes up to 45,000 feet. Its first flight took place during December 2009. Certification to the FAA, EASA, CAAI and TCCA regulations were completed, and type-certificates were obtained. Deliveries began in 2012.

The aircraft is powered by twin Honeywell HTF7250G engines, each producing 7,445 pounds of thrust. The aircraft is capable of nonstop flight from New York to London or from London to Dubai. The aircraft has a very roomy and quiet cabin. The cabin environment includes 100% fresh air and a cabin altitude not exceeding 7,000 feet. Its Design Life Goal (DLG) is 20,000 flights or 36,000 flight-hours.

As part of its damage-tolerance certification program, a structurally complete airframe test-article was fatigue tested for two lifetimes (40,000 flights), followed by half a lifetime (10,000 flights) of damage-tolerance testing

with artificial flaws inflicted at critical locations. Residual strength tests, under limit loads and cabin pressurization, will be performed in the presence of large cracks at several critical locations. This will be followed by a selected teardown inspection.

The test article consists of a structurally complete airframe, including the entire empennage structure. The vertical stabilizer, horizontal stabilizer, elevators, scissors, pivot fitting and dummy horizontal stabilizer trim actuator (HSTA) are included in the fatigue test-article. Figure 3 below shows the fatigue test-article mounted in its loading fixture upon completion of two lifetimes (40,000 flights). Figure 4 shows a schematic view of the fatigue test setup, and showing the loading system.



**Figure 3. Complete Airframe Mounted in its Fixture upon completion of two lifetimes (40,000 flights)**

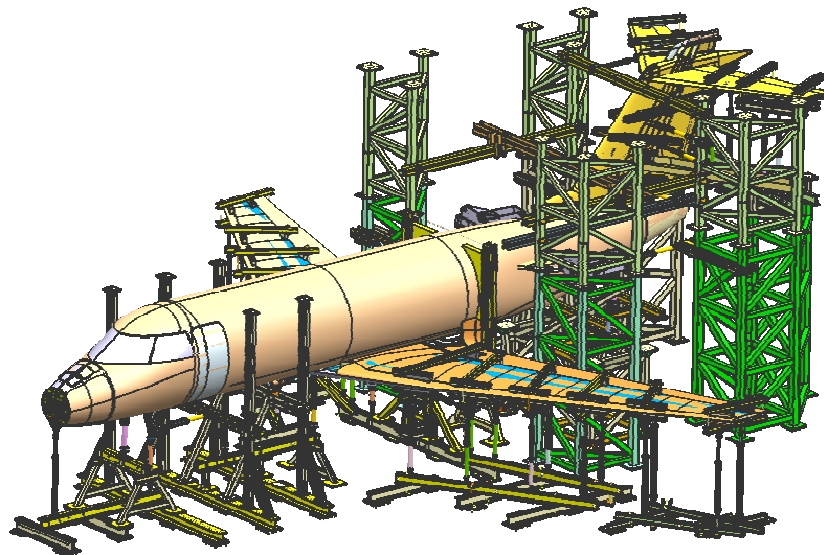


**Figure 4. Schematic View of the Fatigue Test Setup**

The full-scale fatigue test spectrum includes a complete set of symmetric and asymmetric fatigue loads, including engine thrust reverser buffeting loading on the empennage and a suitable representation of engine support loading and main landing gear backup structure loading. The loading spectrum contains 57 cycles per flight (approximately 10-12 minutes per flight). Loads are applied through 58 loading zones and are reacted at six locations. A cabin pressure differential of 9.2 psi is applied during each flight. Periodic inspections for cracks are performed at suitable intervals using various NDI methods. Periodically, a total of more than 1500 strain-gage measurements are recorded, under a set of calibration loads, in order to determine if any significant fatigue damage has occurred at various critical locations. The full scale fatigue test was launched on March, 2011, and completed two lifetimes by March, 2014.

Total of 42 different findings were reported in scheduled inspections during the cyclic testing. These findings were scattered within 23 structural elements in the aircraft. All of these were addressed, and relevant design improvements and retrofits were employed in fleet to ensure the structural integrity of the aircraft. The aircraft maintenance manual was updated accordingly.

At the end of two lifetimes (40,000 flights) of cyclic testing, about 30 artificial flaws were introduced at several critical locations. An example of implementation of artificial crack in the wing front spar lower cap is shown in Figure 5. Impact damages conducted on the horizontal tail composite skin is shown in Figure 6. The damage-tolerance test phase scheduled for another half a lifetime (10,000 flights), in order to ensure that sufficient crack growth data will be obtained. In addition to the artificial flaws, certain cracks detected during fatigue testing were not repaired and their crack growth rates were closely monitored during the damage-tolerance testing. Crack growth gages were installed at crack tips to monitor the growing cracks until the end of the damage-tolerance phase of this test. The damage tolerance phase started on May, 2014, and is expected to complete half lifetime (10,000 flights) by April, 2015.

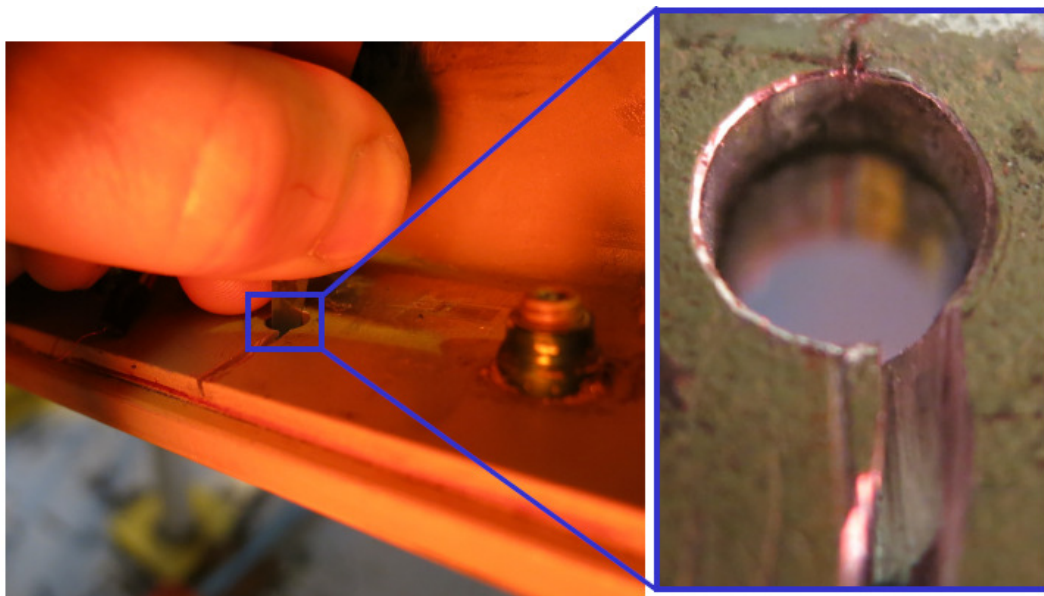


**Figure 5. An example of artificial crack at the wing front spar lower cap**

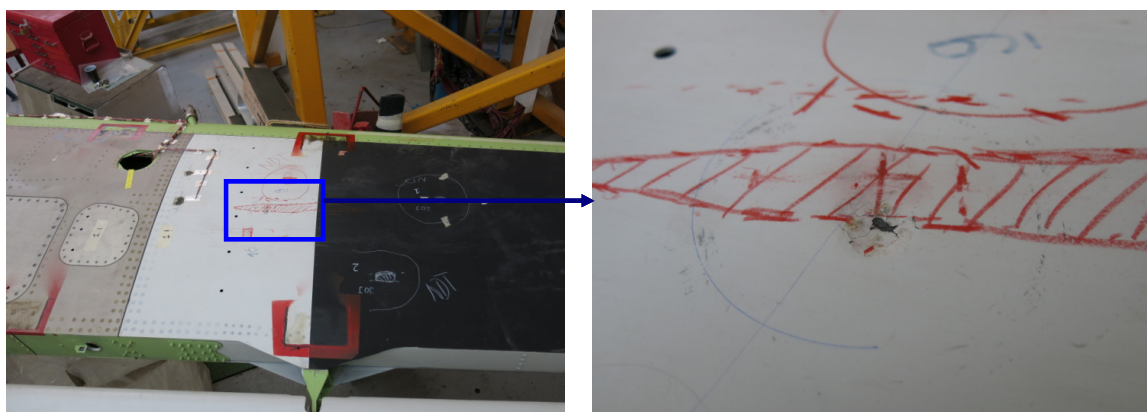


**Figure 6. Impact damage conducted on the horizontal tail composite skin**

At the end of the cycling tests, number of residual strength tests will be performed, including a two-bay crack in the fuselage. Some of the existing cracks will be enlarged significantly before the application of the residual strength loads, to demonstrate that the structure can withstand large discrete source damages.

At the end of the fatigue test, a teardown inspection will be performed, where selected areas of the test-article will be disassembled and inspected for cracks. To date, the test has completed more than 47,000 simulated flights.

### 2.3 IAI Executive Jet, Spoiler Fatigue Test (C. Matias, IAI)

As part of the new IAI executive jet damage-tolerance certification program, the most critical wing Spoiler (among its three spoilers) was fatigue tested for two lifetimes (40,000 flights), followed by residual strength testing with presence of a large crack at its critical location. Teardown inspection and fractographic analyses of the findings were conducted, as well. The test was conducted at Dayton T. Brown (DTB) test facility in Bohemia, New York. It was launched on November, 2011, and completed two lifetimes, the residual strength testing and the teardown inspections by February, 2014.

The test article consists of a full scale production Spoiler assembly supported along the hinge line with production fittings and restrained by a dummy actuator instrumented link. The article is mounted in a test fixture representing the wing aft spar attaching structure. Installation of the test article upon the test fixture is achieved by means of mounted hinge fittings, simulated actuator link calibrated load cells and utilizing production capable hardware. A mechanical test rig supports the test fixture and loading system. To simulate aerodynamic loads, tension pads are bonded to the upper surface of the Spoiler and loaded by an actuator for each pad.

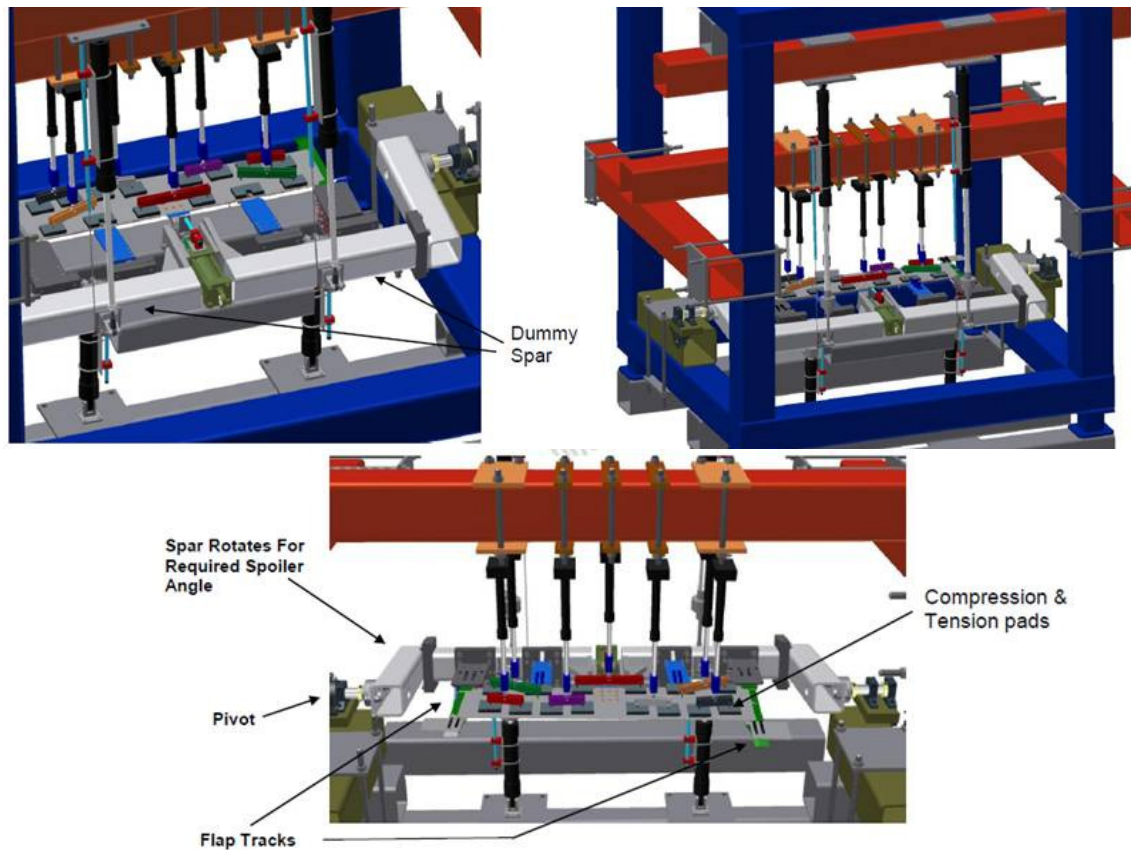
The Spoiler test article is instrumented with strain gauges and position sensors that provide information on the internal loads, hinge reactions, strains in critical locations and measured deflections. The strain gauge data is used to validate the finite element analysis, as well as monitoring the structural integrity of the Spoiler during test. Periodic inspections for cracks were performed at suitable intervals using various NDI methods. More than 150 strain-gauge measurements were recorded, under a set of periodically calibration loads applied, in order to determine if any significant fatigue damage has occurred at various critical structural locations.

Figure 7 shows the Spoiler test-article mounted in its loading fixture upon completion of residual strength test. Figure 8 shows a schematic view of the fatigue test setup, and showing the loading system.



**Figure 7. Spoiler article mounted in test fixture upon completion of residual strength test**

The Residual strength test included application of design limit load on test specimen, with the presence of a nearly critical crack length (that naturally started growing during the fatigue testing). The test specimen withstood the design limit load for three seconds and demonstrated no permanent deformation upon unloading.



**Figure 8. Schematic view of the Spoiler test setup, and the loading system**

#### **2.4 IAI Executive Jet, Flap Fatigue Test (C. Matias, IAI)**

As part of IAI new executive jet damage-tolerance certification program, the most critical wing flap was fatigue tested for two lifetimes (40,000 flights), followed by damage tolerance phase and residual strength testing with presence of a large crack at its critical location. The test is conducted at the National Institute for Aviation Research (NIAR) Full Scale Structural Test Laboratory located in Wichita, KS.

The test article is a full scale production flap assembly. The article is mounted on a test fixture representing the rear spar of the wing box. Aerodynamic loads are applied by load pads and patches bonded to the surface of the flap and loaded by a whiffletree load distribution apparatus. A single wing bending case is applied throughout the duration of the fatigue and damage tolerance portion of the test. A separate wing bending case is being applied for the residual strength test. The flap is instrumented with strain gages. Strain gage data surveys are taken at the beginning of the test and periodically throughout the test in order to monitor the structural integrity of the test article. Additionally, the strain gages data provides information on load distribution and for correlation to the finite element model used for the analyses. Picture of the test article mounted in its test rig is shown in Figure 9.

The test is composed of three stages. First, fatigue test was conducted to two lifetimes, representing 40,000 flights. Next, damage tolerance Test (½ lifetime) is currently being executed, including infliction of discrete damage to the flap in key fatigue sensitive areas. Finally, residual strength test will be performed, by applying the flap design limit load with the presence of crack lengths of “near” the crack growth stability critical crack length to demonstrate residual strength in accordance with FAR 25.571. These critical length cracks can be either spontaneous crack growth or introduced artificially including lengthening of existing spontaneous cracks. In addition, the test includes compliance to FAR 25.671 for presentation of single element failure. Completion of test will be followed by teardown detailed inspections.



**Figure 9. Flap test setup and the loading system**

To date, the flap test had completed its fatigue test phase (two lifetimes) and has started its next phases of the damage tolerance and residual strength tests. Up to now, few cracks were detected at some of the flap tracks roller fittings. All these findings were fully analyzed and design changes were introduced to these items and incorporated into the fleet. The test is expected to be completed by June 2015.

## **2.5 Automated Gust Loads Spectrum for Fatigue Analyses of Aircraft (G. Diamant, Y. Buimovich, IAI)**

Development of gust spectrum of an aircraft is of great concern in aerospace industry. Aircraft structures are subjected to full-scale fatigue testing as part of the certification process. Identification of representative test-load sequences serves an important role in fatigue test definition.

Gust loads encountered by an airplane are defined by means of two methods, i.e. the "discrete" gust concept incorporated in Federal Aviation Regulations (FAR) part 23, and the "continuous" gust concept (methods of power spectral analysis) incorporated in FAR part 25. With the increasing size of aircraft and the associated increasing importance of elastic response, the physical inadequacy of the discrete gust model became apparent and in the early sixties, the continuous turbulence model, using Power Spectral Density (PSD) techniques, was developed.

In this study, an automated application for determination of fatigue spectrum in terms of load factor based on gust PSD model is developed via Excel and Visual Basic. This application is then examined for typical flight cases and compared to results obtained from measured data. In addition, the application developed in this study is compared to another gust PSD Fortran-Based application that was used in the past by the Fatigue and Damage Tolerance Department at IAI.

The case study presented below, was focused on comparing the generated gust exceedance spectrum by the Excel add-in with results published by the University of Dayton Research Institute (UDRI) for Boeing 737-400. The UDRI uses the Power Spectral format (Continuous Gust concept) for the atmospheric turbulence. UDRI has collected data on 17 typical B737-400 aircrafts during operational usage along 11,721 flights representing 19,105 flight hours, corresponding to an overall average of 1.63 flight-hours/flight. The measurements were executed on a single airline. The statistics of operational mission profiles were not recorded. Therefore, for comparison, a single mission profile was developed by the IAI Fatigue and Damage Tolerance Department from

the available statistics. Sixteen Points-In-The-Sky (PITS) were determined, considered as 16 sub-segments of three main segments (Climb, Cruise, and Descent) by using the statistical correlation data from results published by UDRI, corresponding to a 50% probability of occurrence. The Gust exceedance, as well as the load factor spectra comparison results, shown hereinafter of FORTRAN program versus Excel add-in were built based on these PITS. In addition, the results are compared with measured spectrum shown in Figure 10 which provides cumulative occurrence of incremental gust load factor per 1000 hours for combined flight phases.

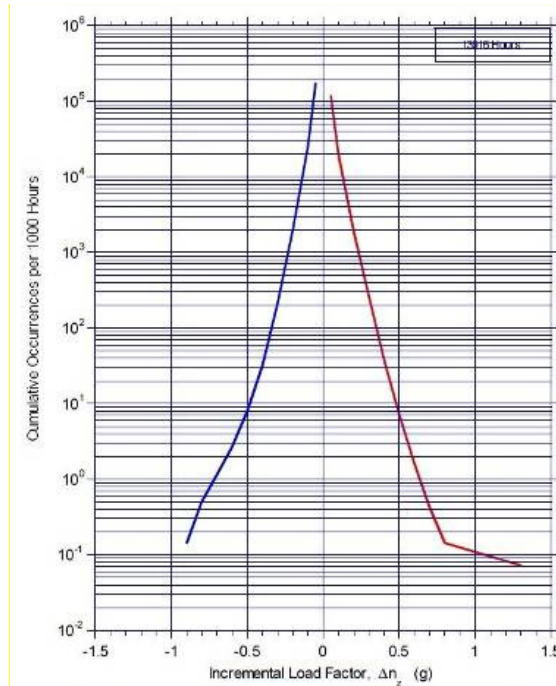


**Figure 10. B737-400 Cumulative occurrence of incremental vertical gust load factor per 1000 hours, combined flight phases**

It may be observed in Figure 11 that the FORTRAN program has generated the most conservational spectrum of incremental gust loads. Whereas the measured one is the most un-conservational, the spectrum generated by Excel add-in is seen to be somewhere between these two curves and preferable as compared to the curve obtained from the FORTRAN program. The results obtained by the FORTRAN application are higher in approximately 20% and 70% than those obtained in the Excel add-in and the UDRI, respectively.

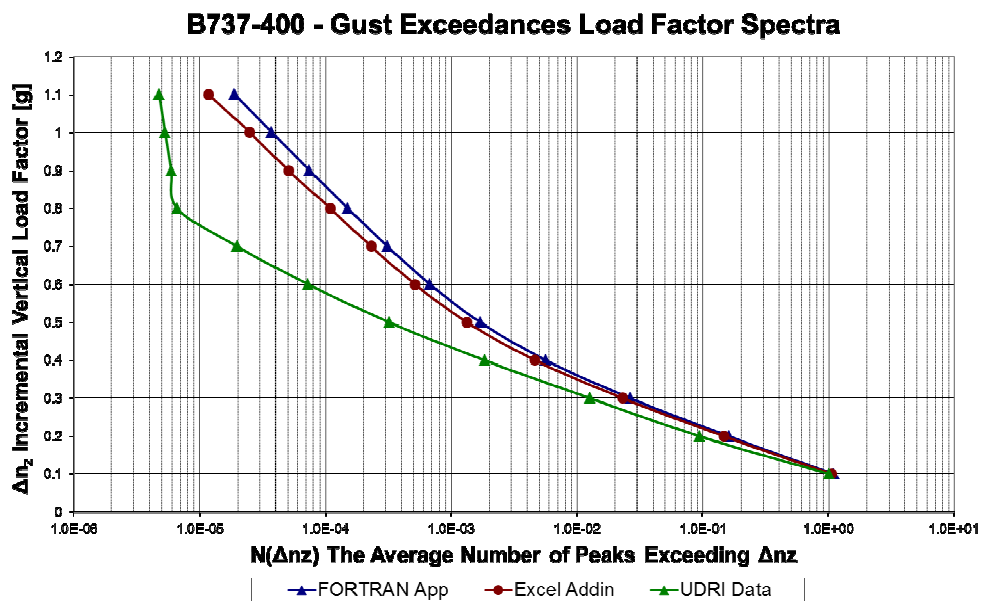


**Figure 11. B737-400 – Gust exceedance, comparison of load factor spectra**

One of the most noticeable improvements in generating the gust exceedance spectrum through the Excel add-in application was shown in terms of generating more precise and hence less conservative gust exceedance spectrum, as compared to the FORTRAN program. This is mainly because the Excel add-in application is based upon more sophisticated data regression techniques and precise derivation of data from graphs of important relevant parameters. Comparison with spectra based on measured data assured that the Excel add-in generates sufficient gust exceedance spectra that are within reasonable range and not exceed realistic data records. Improved and less severe gust exceedance spectra highly influences the design process of an aircraft; because of the relation between the fatigue and damage tolerance analyses and the design requirements compliance such as maintainability, operational life and weight.

A full length paper describing the derivation of load factor spectrum, determination of important relevant parameters and detailed examination of the automated application for fatigue spectrum development may be found in Ref. [9].

## 2.6 Examination of the Influence of Flap Peening Process on the Fatigue Life of Straightened Metal Elements (C. Zur, Y. Buimovich, Y. Freed, S. Ramati)

The flap peening process is widely used for straightening bent metal parts. Although it is usually considered as a life enhancement method, when flap peening is employed to restore the original contour of the part, its effect on the fatigue life of the metallic part should be examined due to possible implementation of moderate tensile residual stresses in the vicinity of fatigue critical locations which already exist in the structural detail. This study presents an experimental investigation of this topic.

Total of 30 open hole specimens made of AL7075-T6 were tested. Two types of specimens were examined in this investigation. The first was an open-hole specimen (without application of flap peening) that served as a reference. The second was an open-hole specimen that was bent via rolling procedure and then straightened by application of flap peening. These specimens were divided into two groups, in which the hole was drilled before and after application of flap peening.

This study focuses on both crack nucleation and complete failure stages. Comparisons between the flap peened specimens and the references specimens are graphically illustrated by means of average number of cycles at fracture in Figure 12 and Figure 13, for specimens with thickness of 1.5 mm and 3.2 mm, respectively. In addition, comparative illustrations of the portions of crack nucleation out of the total lifetime are graphically presented in Figure 14 and Figure 15. That is, the ratio between the number of cycles at crack nucleation and the number of cycles up to failure (red rectangles) is presented. Also, an average value of the number of cycles at crack nucleation is graphically shown in these figures by a dashed orange line.

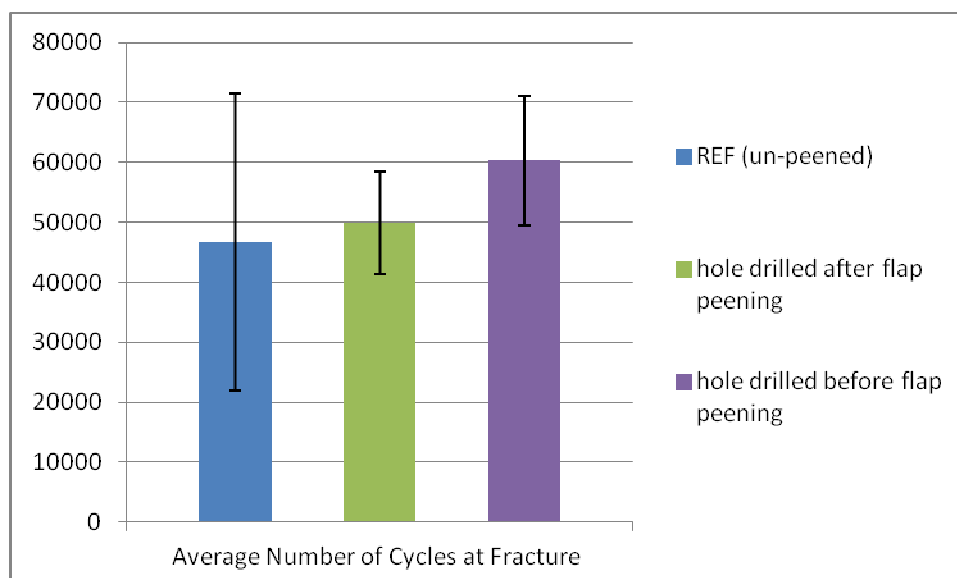


**Figure 12. Comparison of the average number of cycles at failure of specimens with thickness of 1.5 mm, length of 400 mm**

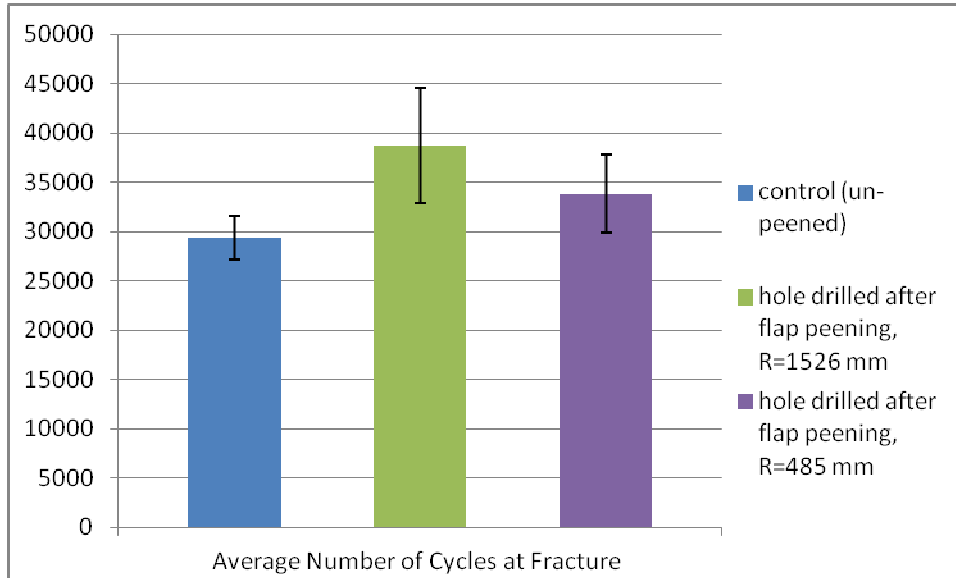


**Figure 13: Comparison of the average number of cycles at failure of specimens with thickness of 3.2 mm, length of 300 mm**

It may be observed in Figure 12 that the standard deviation of the reference batch was highly affected by an exceptional value of the number of cycles up to failure of one of its specimens. Although taking it into account, the average number of cycles at fracture is still lower as compared to those that related to the flap peened specimens. It may be seen that the average number of cycles of the specimens in which the hole is drilled before the flap peening is much larger than that of the specimens in which the hole is drilled after the flap peening. An improvement in the fatigue life of the flap-peened specimens is observed in Figure 13 (with respect to the un-peened specimens). Comparison of the two different radii of curvature shows that the average number of cycles up to failure of the specimens with the greater radius is greater and that those specimens usually possess higher fatigue lives.

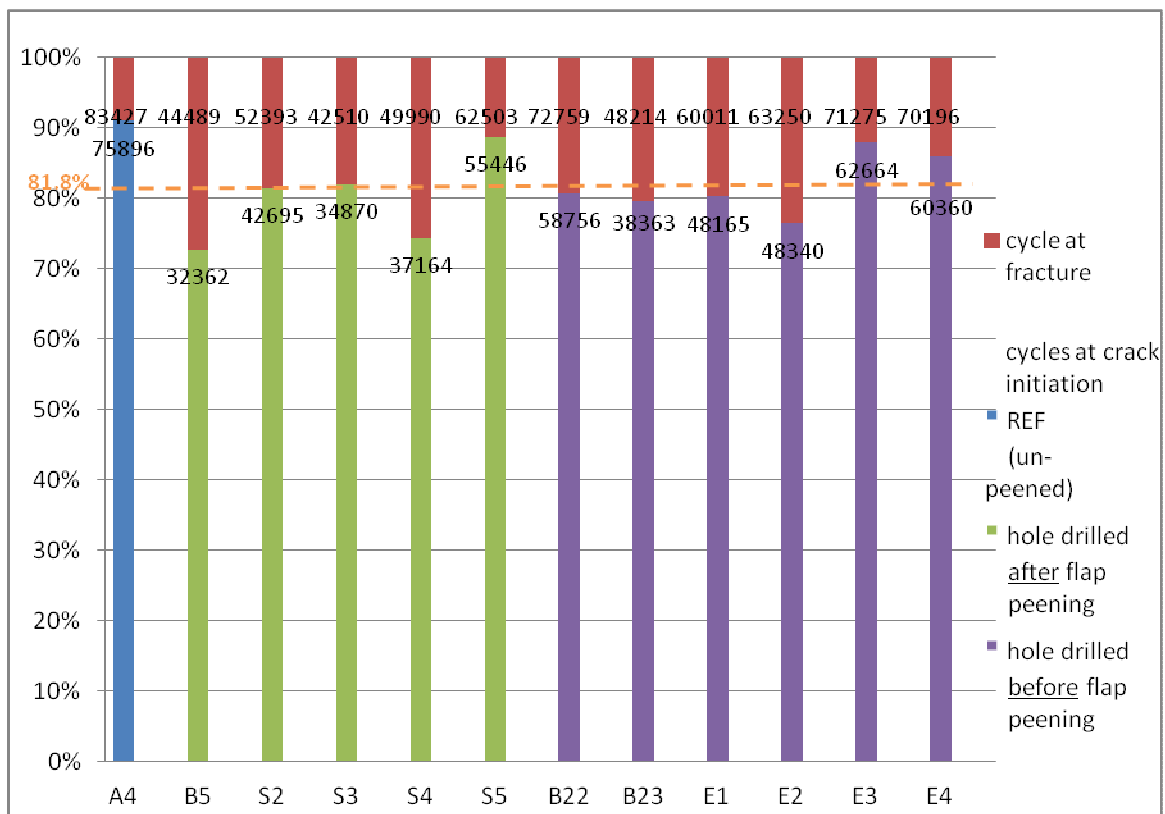


**Figure 14: Percentage of crack initiation out of failure of specimens with thickness of 1.5 mm, length of 400 mm**

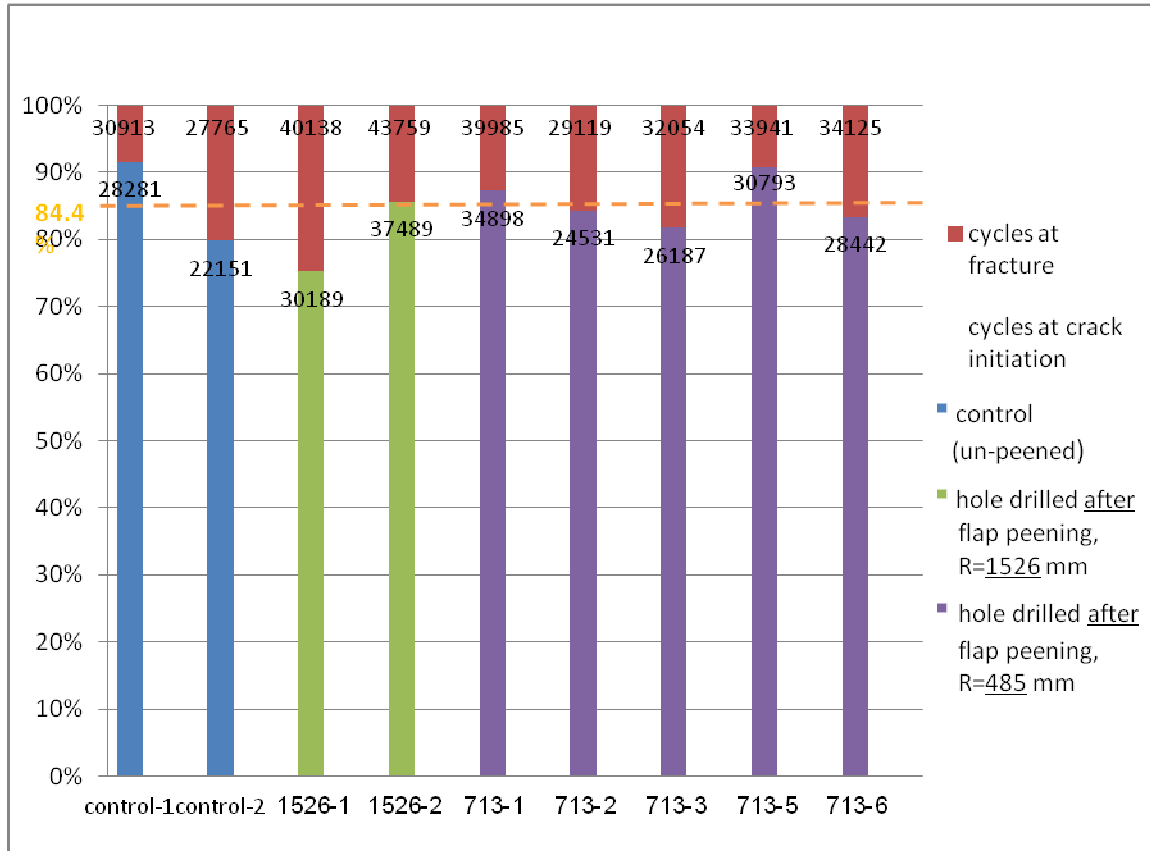


**Figure 15: Percentage of crack initiation out of failure of specimens with thickness of 3.2 mm, length of 300 mm**

To conclude, it was shown that the fatigue life of bent specimens that were straightened by flap peening is greater than the fatigue life obtained for the reference specimens, which were not bent nor peened. Hence, the flap peening process indeed improves the fatigue life of bent metal elements that were straightened through this procedure.

A full length paper describing the all test findings and conclusions may be found in Ref. [10].

### 2.7 An Improved Method for Calculating the "Fatigue Strength Reduction Factor" ( $K_f$ ) for Fatigue Life Analysis (A.Brot, IAI)

S-N diagrams are usually constructed to provide fatigue life data for a specific alloy, a specific product form (sheet, plate, forging, etc.) a specific direction of loading, and for a specific stress-concentration factor ( $K_t$ ). Each diagram contains several curves, corresponding to the various mean stresses that were tested. To fully account for various stress-concentrations and mean-stress conditions, 400 – 500 specimens must be tested for each alloy, to provide sufficient data and to neutralize the large scatter inherent in fatigue testing. Some of the specimens will need to be tested for more than 10 million cycles. The "MMPDS Handbook", administered by the FAA, contains a large database of S-N diagrams for many alloys used in the aerospace structures, which were obtained by testing a very large number of test specimens.

At the 54th Israel Annual Conference on Aerospace Sciences, the author presented a paper describing a study that could reduce the number of test specimens needed to define the fatigue properties of an alloy [11]. It was found in the previous study, that using the "fatigue strength reduction factor" ( $K_f$ ) instead of the "stress concentration factor" ( $K_t$ ) could greatly reduce the number of required specimens. In addition, two methods for accounting for mean stress effects were evaluated by using two types of software and the S-N data. The previous study showed that the Neuber Equation gave unsatisfactory results, and a modified Neuber Equation was proposed [11]:

$$K_{Nm} = 1 + \frac{K_m - 1}{1 + 2\sqrt{A}/\sqrt{r}}$$

It was shown in [11] that the modified Neuber Equation gave more satisfactory results compared to the MMPDS S-N data. It appears that the Neuber Equation, which apparently was formulated intuitively, needs to be examined in more detail in order to possibly restructure its formulation.

The present study has abandoned both the original Neuber equation and the modified Neuber equation and attempts to determine the relationship between the fatigue strength reduction factor ( $K_f$ ) and the stress-concentration factor ( $K_{tn}$ ) without the use of the Neuber equation. The following shows, schematically, the modified approach for 2024-T3 aluminum alloy:

- The entire cycle scale of the S-N diagram was broken down into four values that cover the entire practical range: 10,000 cycles, 40,000 cycles, 160,000 cycles and 640,000 cycles.
- For each value of  $K_{tn}$  that appears in the MMPDS, S-N diagram (1.5, 2.0, 4.0 and 5.0) for 2024-T3 alloy, the maximum stresses (at  $R = -1$ ) that result in the above four values of life, were obtained from MMPDS.
- Values for  $K_{tn} = 3.0$  were added by curve-fitting cross-plotted data.
- GlyphWorks software was then run for each value of maximum stress (at  $R = -1$ ), and  $K_f$  was determined to corresponds to the MMPDS fatigue life.
- In this way, the relationship between  $K_{tn}$ ,  $K_f$  and stress level was determined for 2024-T3 alloy, without needing to use the original or modified Neuber Equation.

Figure 16 shows graphically variation of  $K_f$  as a function of the maximum stress level, including the corresponding values of  $K_{Nm}$  that was developed in [11], which is not a function of the applied stress.

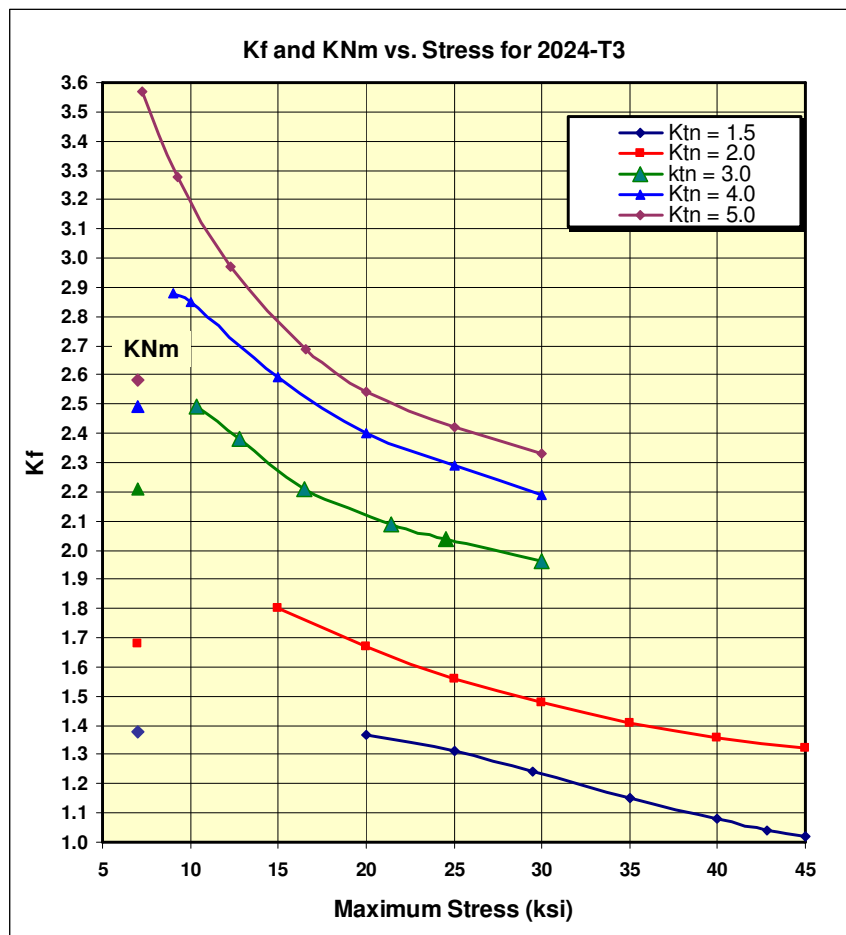


Figure 16. Determining  $K_f$  for 2024-T3 alloy based on  $K_{tn}$  and maximum stress level

Using the data shown in Figure 16 for 2024-T3 alloy, one can determine the appropriate value of  $K_f$  to be used in a GlyphWorks run as a function of both  $K_{tn}$  and the maximum stress level. It should be noted that for spectrum loading, each layer in the spectrum will have a different value of  $K_f$ .

Figure 17 and Figure 18 confirm the accuracy of this method by comparing MMPDS and GlyphWorks results for specific loading at  $R = 0$  and  $R = -1$ .

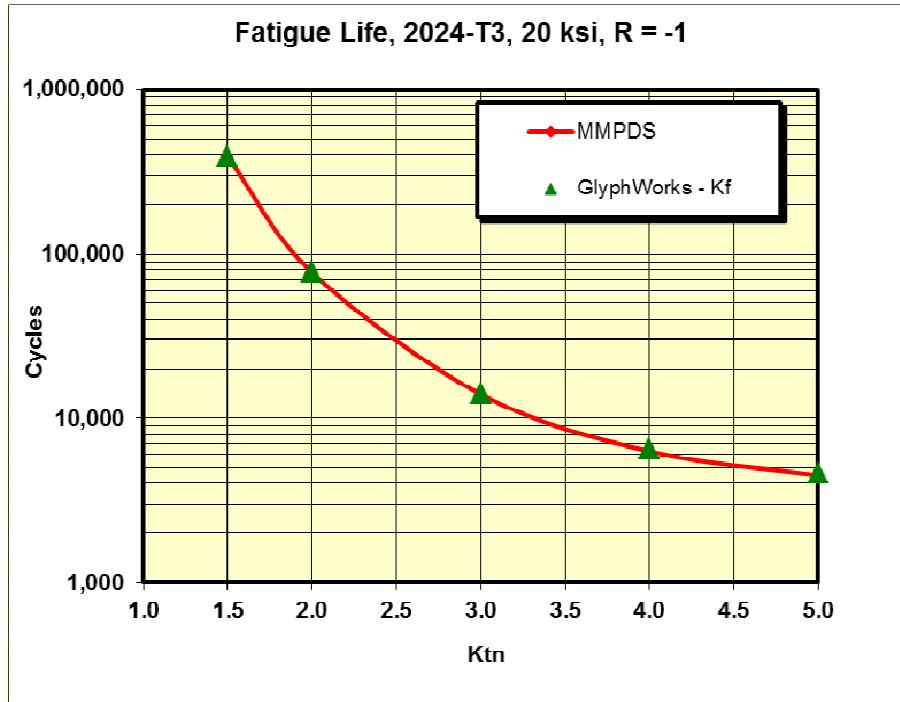


Figure 17. Comparison of results for 2024-T3 alloy at  $R = -1$

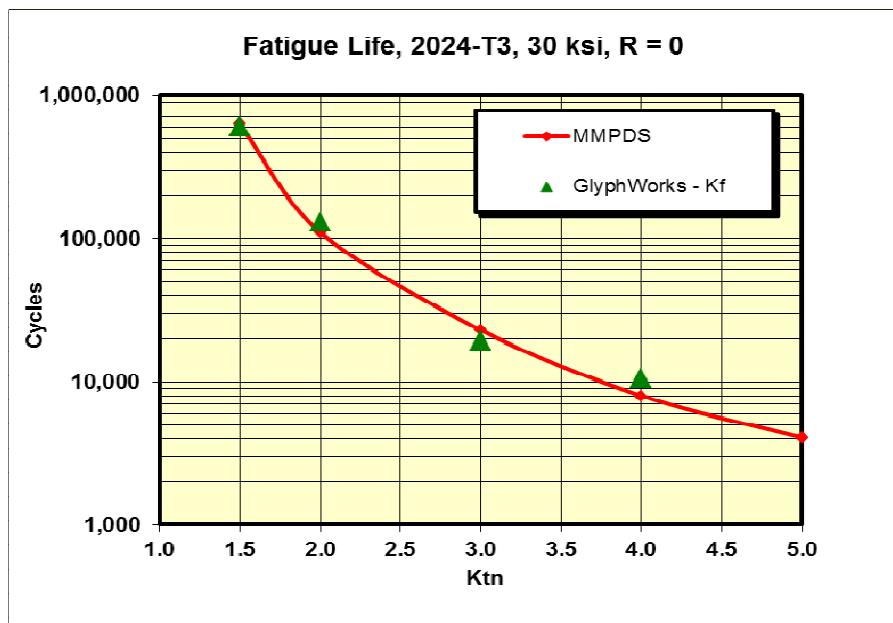


Figure 18. Comparison of results for 2024-T3 alloy at  $R = 0$

## 2.8 Mutual Influence of Two Opposing Cracks at a Hole (C. Matias, A. Brot, G. Noivirt, C. Zur, Y. Amran, IAI)

The safety of "normal" repeated cyclic flight operations (i.e. no emergency conditions), considering structural integrity, is provided by the fatigue and damage tolerance analyses and substantiations. The aim of these analyses is to show that the airframe will have adequate residual strength (to withstand rare loading conditions such as some emergency conditions) in the presence of flaws or cracks subjected to crack growth under "normal" operating conditions, for the entire operational service usage life. Under this philosophy, routine periodic inspections will detect the cracks before failure. Under damage tolerance methodology, flaws are assumed to exist initially in the structure as a result of the manufacturing process, normal usage and maintenance operation.

As it is virtually impossible to specify and analytically model all the types and sizes of initial defects and flaws that might exist in aircraft structures, it is common practice in the industry to assume specific initial crack sizes and shapes to serve as the surrogates for all of these possible types of defects.

For relatively large cracks, it is evident that cracks nucleating simultaneously from both sides of the fastener hole, as depicted in Figure 19, in which a fractographic analysis results of fatigue crack growth in an aircraft main beam during full-scale fatigue test are presented.

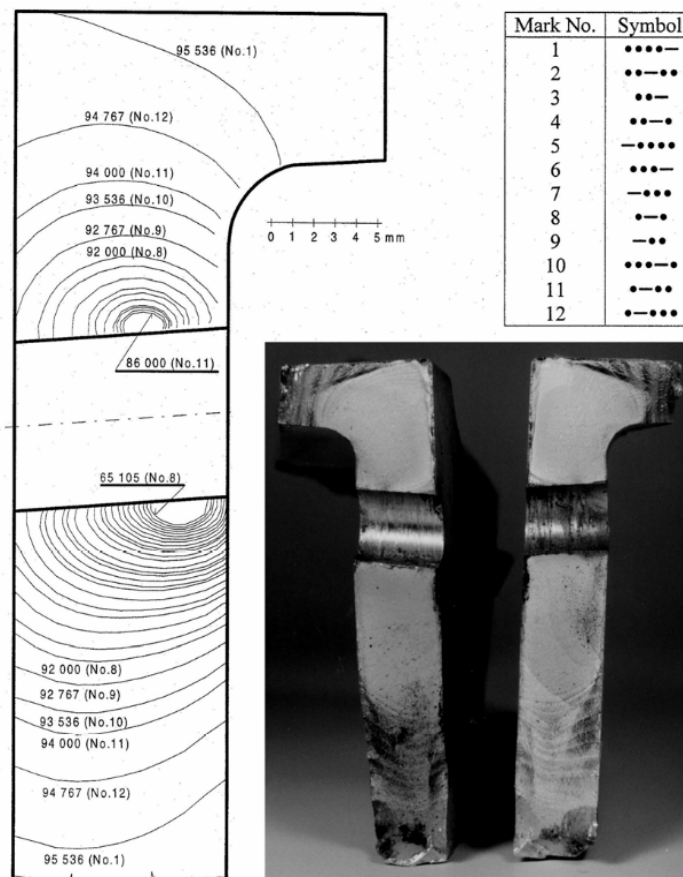


**Figure 19. Simultaneous crack growth at two opposite sides of fastener hole [17]**

In standard crack growth analyses it is not a common practice to account for the mutual effect between the two crack tips emerging from the same fastener hole. This common practice was done mainly due to the lack of adequate computing codes. Without such proper computing codes accounting for this mutual influence, it can only be done as an iterative process. This process will be very tedious and time consuming, so it was rarely done. However, as it is shown in this study, using NASGRO ver. 7.1 [18], which has the capability of accounting for these mutual effects, neglecting this mutual influence will lead to somewhat un-conservative analyses results. This is of special interest when analyzing widespread fatigue damage crack growth scenarios, in which multiple cracks nucleate from adjacent fastener holes.

A full length paper describing the all test findings and conclusions may be found in Ref. [19].

## 2.9 Investigations on the Bauschinger Effect and Induced Stress Intensity Factors of Erosion Cracking in Autofrettage Cylindrical Pressure Vessels (Q. MA, C. Levy, M. Perl, J. Perry, BGU)

For the investigation of cracked problems in thick-walled pressurized cylindrical vessels, the displacement-based finite element method has become one of the main computational tools to extract stress intensity results for their fatigue life predictions. The process of autofrettage, practically from the partial autofrettage level of 30% to full autofrettage level of 100%, is known to introduce favorable compressive residual hoop stresses at the cylinder bore in order to increase its service life. In order to extract the fatigue life, stress intensity factors (SIFs) need to be obtained a priori.

The necessity for determining SIFs and their practical importance are well understood. However, it is usually not a trivial task to obtain the required SIFs since the SIFs largely depend on not only the external loading scenarios, but also the geometrical configurations of the cylinder. In recent studies it was shown that the Bauschinger effect (BE) may come into play and affect the effective SIFs significantly for an eroded fully autofrettaged thick-walled cylinder. In this study, the authors further investigate the SIFs for the Bauschinger effect dependent autofrettage (BEDA) and the Bauschinger effect independent autofrettage (BEIA) at various autofrettage levels.

The crack is considered to emanate from the erosion's deepest point in a multiply eroded cylinder. The commercial finite element package, ANSYS ver. 12, was employed to perform the necessary analysis. A two-dimensional model, analogous to the authors' previous studies, has been adopted for this investigation. The residual stress field of autofrettage process, based on von Mises yield criterion, is simulated by thermal loading. The combined SIFs are evaluated for a variety of relative crack lengths with cracks emanating from the tip of erosions with various geometrical configurations and span angles. Figure 20 illustrates the induced residual plastic strains for different radii ratios  $W$ . The effective SIFs for relatively short cracks are found to be increased by the presence of the erosion and further increased due to the BE at the same autofrettage level, which may result in a significant decrease in the vessel's fatigue life. Deep cracks are found to be almost unaffected by the erosion, but may be considerably affected by BE as well as by the level of partial autofrettage.

Full details on these studies are provided in Refs. [24, 25 and 27].

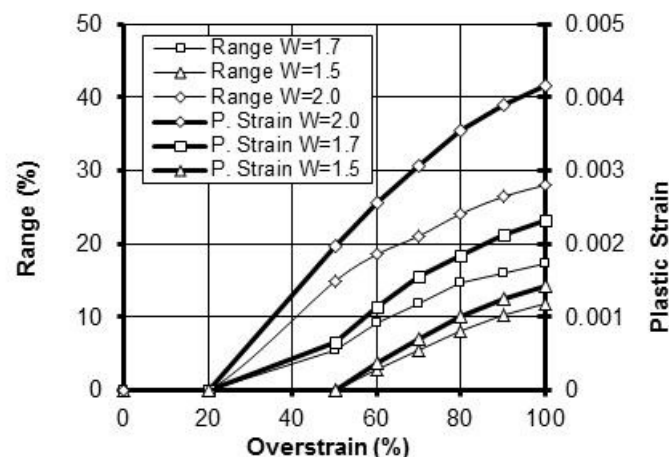


Figure 20. Barrel safe maximum pressure range and residual plastic strain vs. overstrain levels for different radii ratios  $W$ .

## 2.10 3-D Stress Intensity Factors due to Autofrettage for an Inner Radial Lunular or Crescentic Crack in a Spherical Pressure Vessel (M. Perl, M. Steiner, J. Perry, BGU)

Spherical pressure vessels, though less common than cylindrical ones, are widely used in industry mainly due to their optimal specific strength (strength/weight) and their ease of packing. Spherical pressure vessels are used,



for example, as propellant/oxidizer/pneumatic tanks on space-crafts and aircrafts, storage tanks for pressurized chemical substances, gas tanks on LNG (liquefied natural gas) carriers, cookers for the food industry, and as containment structures in nuclear power plants. Moreover, whenever extremely high pressure occurs, such as in high explosion containment tanks, or in the apparatus used to manufacture artificial diamonds and other crystals, spherical pressure vessels is literally the only feasible solution.

Some of these spherical pressure vessels are manufactured from a series of double curved petals welded along their meridional lines. These pressure vessels are susceptible to cracking along the welds due to one or more of the following factors: cyclic pressurization-depressurization, the existence of a heat-affected zone near the welds, tensile residual stresses within this region, and the presence of corrosive agents. As a result, one or more radial cracks develop from the inner surface of the vessel on the welding planes.

Three dimensional Mode I Stress Intensity Factor (SIF) distributions along the front of an inner radial lunular or crescentic crack emanating from the bore of an autofrettagged spherical pressure vessel are evaluated. A 3-D analysis is performed using the finite element (FE) method employing singular elements along the crack front. A novel realistic autofrettage residual stress field incorporating the Bauschinger effect is applied to the vessel.

The residual stress field is simulated in the FE analysis using an equivalent temperature field. SIFs for three vessel geometries ( $R_0/R_i=1.1, 1.2, \text{ and } 1.7$ ), a wide range of crack depth to wall thickness ratios ( $a/t=0.01-0.8$ ), various ellipticities ( $a/c=0.2-1.5$ ), and three levels of autofrettage ( $e=50\%, 75\% \text{ and } 100\%$ ) are evaluated. In total, about two hundred and seventy different crack configurations are analyzed. A detailed study of the influence of the above parameters on the prevailing SIF is conducted. The results clearly indicate the possible favorable effect of autofrettage in considerably reducing the prevailing effective stress intensity factor, i.e., delaying crack initiation, slowing crack growth rate, and thus, substantially prolonging the total fatigue life of the vessel. Furthermore, the results emphasize the importance of properly accounting for the Bauschinger effect including re-yielding, as well as the significance of the three dimensional analysis herein performed.

Full details on this study are provided in Ref. [26].

## **2.11 Unified Fatigue modeling in metals (M.P. Weiss, Technion)**

A unified model that combines the classical fatigue studies and results with fracture mechanics approach has been introduced in Ref. [49]. The model included both approaches in one diagram, depicted in Figure 21.

The fatigue domain has been split into six different fatigue regimes, each with unique fatigue behavior and calculation procedure. The main parameters of the model are the crack length and the engineering stress amplitudes, even in very small cracks. The fatigue damage has not been contemplated. Instead of trying to find one relation that may enable to predict fatigue behavior, separate relations for each zone have been considered. Later additional studies that enhanced the proposed diagram and method have been reported, for two stress level loading [50], for consideration of mean stresses [51], for application in fatigue of wire ropes [52], and others.

In the current study the diagram has been changed to use the remote stress amplitude, that is more convenient for application, and the model was updated to consider surface finish of the material. The study has been completed and is in stages of preparation to be submitted for publication [53].

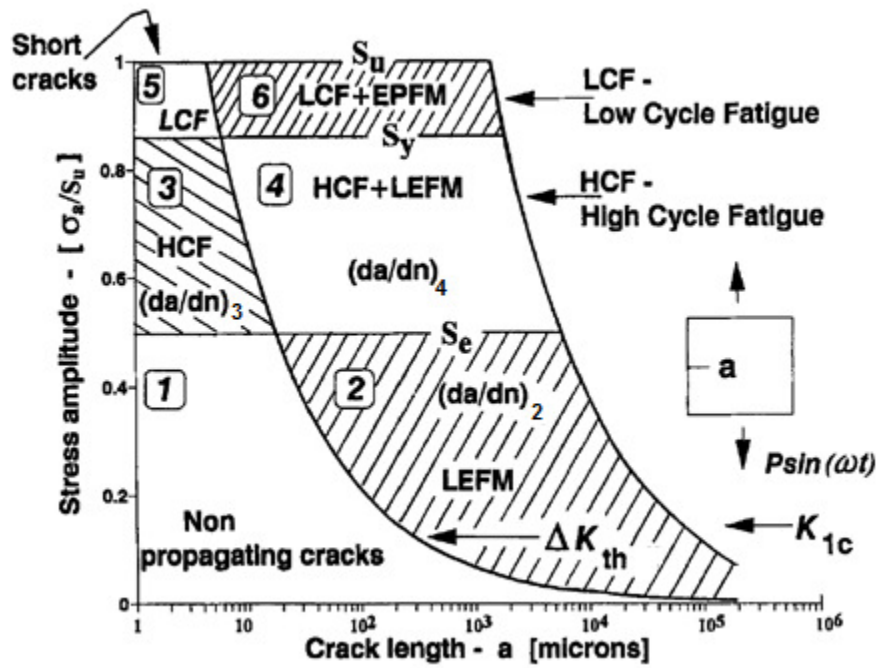


Figure 21. The unified fatigue diagram that splits the whole fatigue domain into 6 zones

### 3. STRUCTURAL INTEGRITY OF COMPOSITE MATERIALS

#### 3.1 Accelerated Testing Methodology for the Predictions of Long Term Strength and Durability of Composite Materials in a Marine Environment (Y. Freed, Y. Buimovich, IAI)

This activity is a continuation of an activity that was reported in the 2013 Israel National Review [1].

It is well known that the strength and the durability of air vehicles made of composite materials strongly degrade when utilized in marine environment (exposed to varying temperatures and moisture). With the increase use of composite materials as primary structures in light-weight unmanned air vehicles that operates intensively in a marine environment, the ability to predict long term behavior of composite materials becomes essential. Since modern aircraft are designed to operate for 30 – 40 years, it is needed to establish an accelerating testing methodology that can be employed in determination of material design allowables and can even replace long-term testing.

Most of aviation products made of composite materials are certified using AC 20-107B methodology, in which "the effects of repeated loading and environmental exposure which may result in material degradation should be addressed in the static evaluation..." and "Fatigue substantiation should be accomplished by... accounting for the effects of the appropriate environment". The common approach to account for the environmental effect is to perform hot-wet coupon tests or, alternatively, reduce the material strength and fatigue allowables (or increasing the applied loads) by a certain level. For instance, MIL-HDBK 17 recommends applying a load enhancement factor of 1.06 as an environmental compensation factor. This is certainly a conservative approach that can be employed when no other relevant engineering data is available.

In this study, an accelerating testing methodology for the determination of residual strength and durability degradation of the composite material upon time is introduced. This method was originally developed to determine non-destructive material properties of polymers, but it can be shown that it may be applicable to certain types of composite materials as well [5]. The basic idea of this method is to perform viscoelastic testing at several elevated temperature and water absorption states to obtain the relation between the temperature, the moisture and the testing time periods. This relation, usually referred to as a 'Time-Temperature-Moisture Superposition Principle' (TTMSP), holds for creep, residual strength, and fatigue behavior of the unidirectional composite material, under certain limitations. With additional sets of simple constant strain-rate and fatigue coupon tests, the environmental effect on the mechanical properties of the composite material can be determined. This procedure is schematically described in Figure 22.

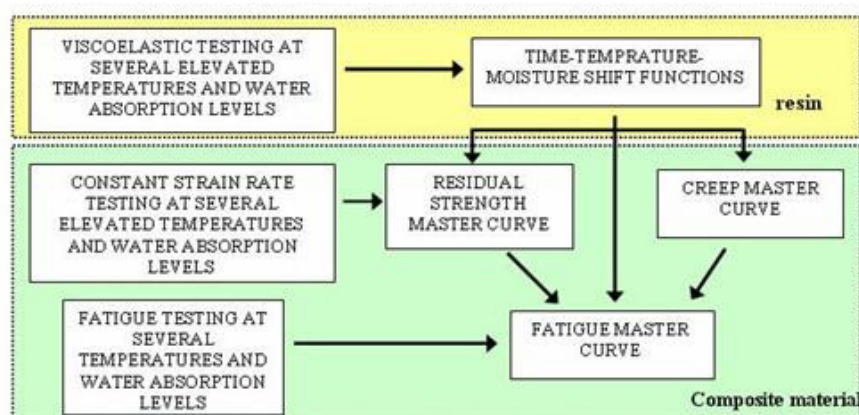


Figure 22. Schematic description of the accelerating testing methodology.

The outcome of this study is a set of master-curves, in which the long term behavior of the composite material is described in terms of applied loads, number of cycles to failure, load frequencies, and operational temperatures and moisture levels. Both three point bending and tensile specimens are tested.

The final results were presented as an oral presentation in the 16<sup>th</sup> Israeli Conference of Composite Materials and Structures in 2013. An example of typical fatigue master curve is shown in Figure 23.

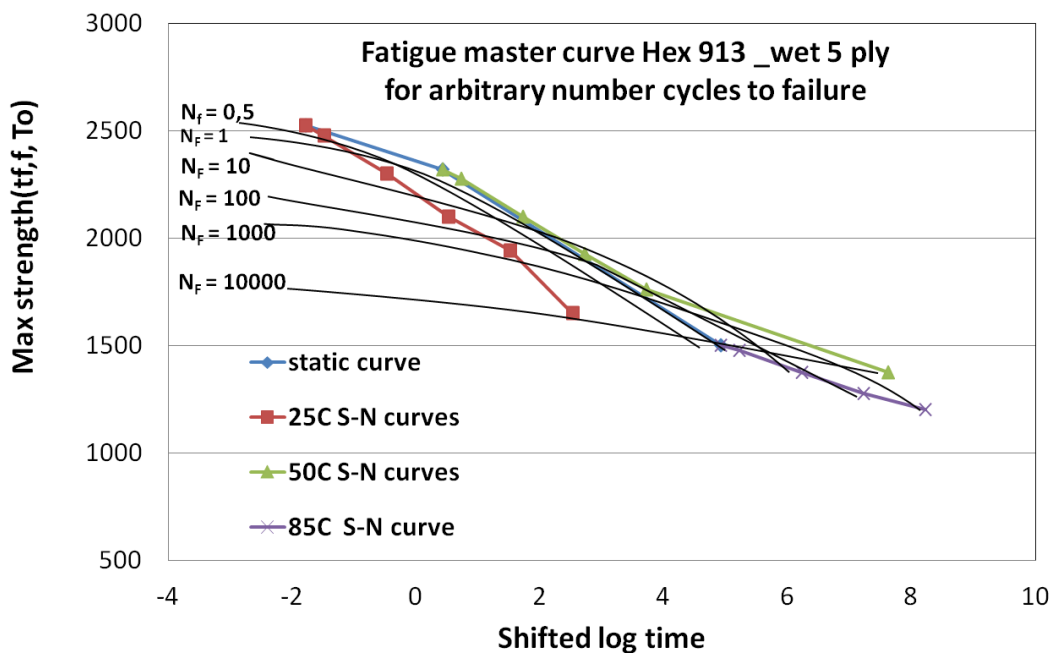


Figure 23. Fatigue flexural bending master-curve in a moist environment.

### 3.2 Review of Methods to Substantiate Aeronautical Structures Made of Composite Materials to Its Expected Lifetime (N.Y. Shemesh, E. Harris, S. Nissim, IAF)

Composite materials are well known for their superior fatigue properties. The common assumption, which is widely adopted as a conservative design criterion, is that as long as the strain levels in the structure are sufficiently low, the structure is not prone to fatigue cracking. However, the main disadvantage of composite materials lies in their poor resistance to out of plane loads, and their sensitivity to manufacture and impact damage in service. Field experience in Israel Air-Force showed, as opposed to common perception, that damages do grow in bonded composite structures. In addition, the civil regulation standards and the emerging Unmanned Air Vehicles (UAVs) regulation standard (STANAG 4671) require the designer to demonstrate the damage tolerance capability of the structure. In other words, the designer must show that the presence of imperfection or damages in the structure will not reduce its residual strength during its expected lifetime, taking into account the cyclic loads in which the structure is subjected to.

The continuing operation of UAV platforms in Israel Air-Force requires developing substantiation methods to determine the UAV expected lifetime and corresponding maintenance plan, in light of developments in regulation standard that are commonly used in the world. Moreover, development of such computational methods to determine fatigue lifetime will improve and enrich material databases available in Israel, as well as knowledge on performance of composite materials upon cyclic loads. These activities can save costs by reducing tests early at the platform phase while meeting the customer requirements and provide solutions to in-service findings in Israel Air-Force fleet.

This review was presented in The 16th Conference of Composite Materials and Structures in 2013.

### 3.3. Mode I and Mode II fracture energy of MWCNT reinforced nanofibrilmats interleaved carbon/epoxy laminates (S. Hamer, IAI, D. Sherman, Technion)

It is well established that Multi Wall Carbon Nano-Tubes (MWCNTs) implemented in composite materials can improve its overall strength, fracture toughness and crack propagation properties. Once this promising technology become mature, it can be implemented in aerospace, military and automobile applications.

In this study, laboratory scale carbon/epoxy laminates were interleaved with electrospun Nylon 66 nanofibrilmat reinforced with MWCNTs. The effect of the MWCNTs on the fracture energy was evaluated under Mode I and Mode II loading. It is shown that while nanofibrilmat interleaving resulted in a three times increase of the Mode I fracture energy compared to the non-interleaved laminates and the MWCNT reinforced nanofibrilmat interleaving resulted in a four times increase (Figure 24). Evaluation of the Mode II fracture energy indicated a 40% increase as a result of nanofibrilmats interleaving, while MWCNT reinforced nanofibrilmat interleaving resulted in a 60% increase (Figure 25). Mechanisms for the fracture energy increase of the MWCNT reinforced nanofibrilmats are suggested based on the test data and fractographic study of post-test specimen surfaces.

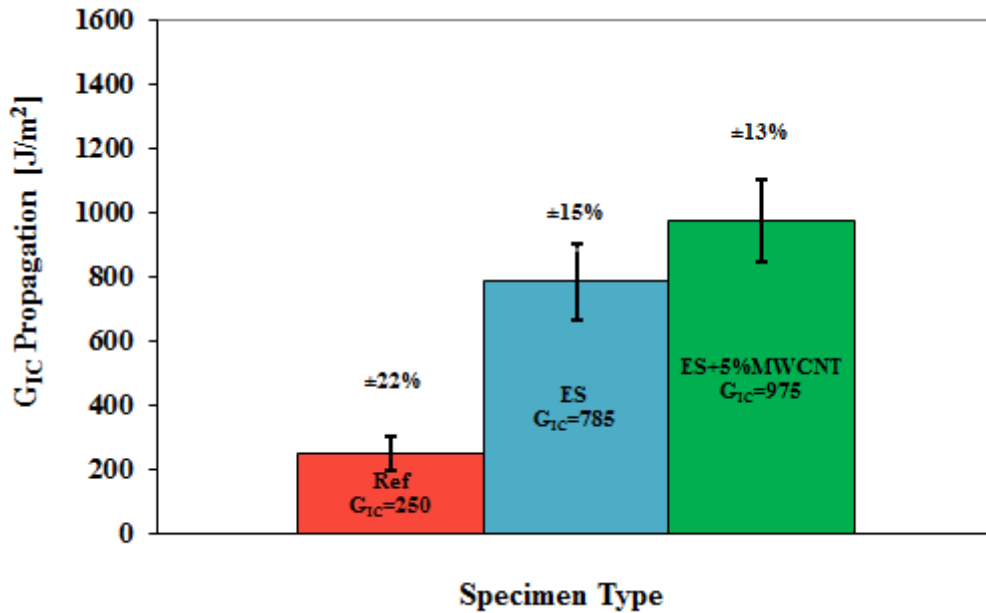


Figure 24. Comparison of mode I fracture energies  $G_{IC}$  with and without MWCNT reinforcement.

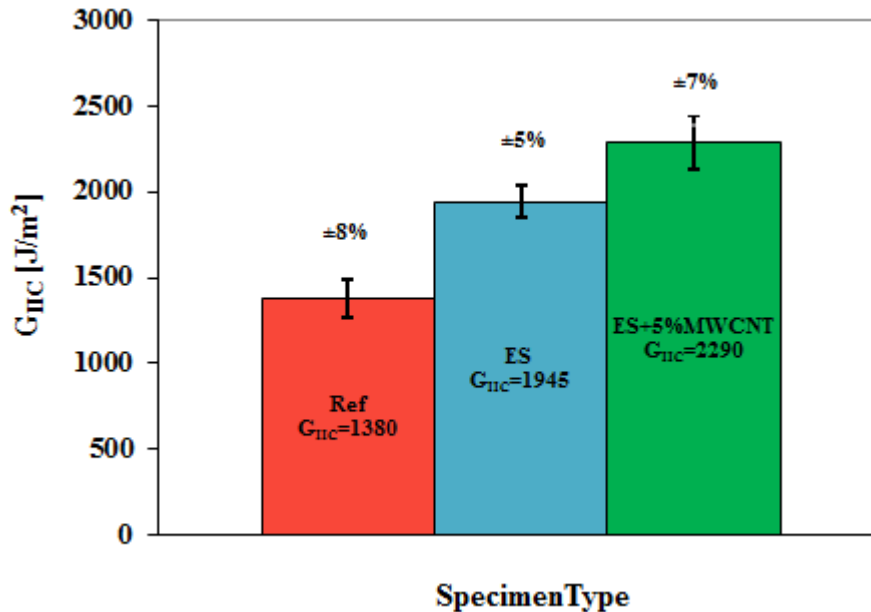


Figure 25. Comparison of mode II fracture energies  $G_{IIc}$  with and without MWCNT reinforcement.

More details on this study are provided in Ref. [28].

### 3.4 Progress Report at the Mechanics of Composite Materials Lab (R. Haj-Ali, TAU)

The overall goal of the Mechanics of Composite Materials (MCM) Lab at Tel-Aviv University (TAU) is to conduct analytical-computational and experimental scientific research in the general area of mechanics of composite materials and structures. Over the last two years, the MCM lab has been engaged in the following research projects:

- 1) Micromechanical modeling of composites: A new 3D parametric high fidelity generalized method of cells (HFGMC), Ref. [47] - A 2D and 3D parametric formulation of the high fidelity generalized method of cells (HFGMC) is generalized for the micromechanical analysis of three-dimensional (3D) multiphase composites with periodic microstructure. Several applications for 3D composites are presented to demonstrate the general capability and varsity of the parametric HFGMC method for refined micromechanical analysis as seen in Figure 26 for the spatial distributions of local stress fields.

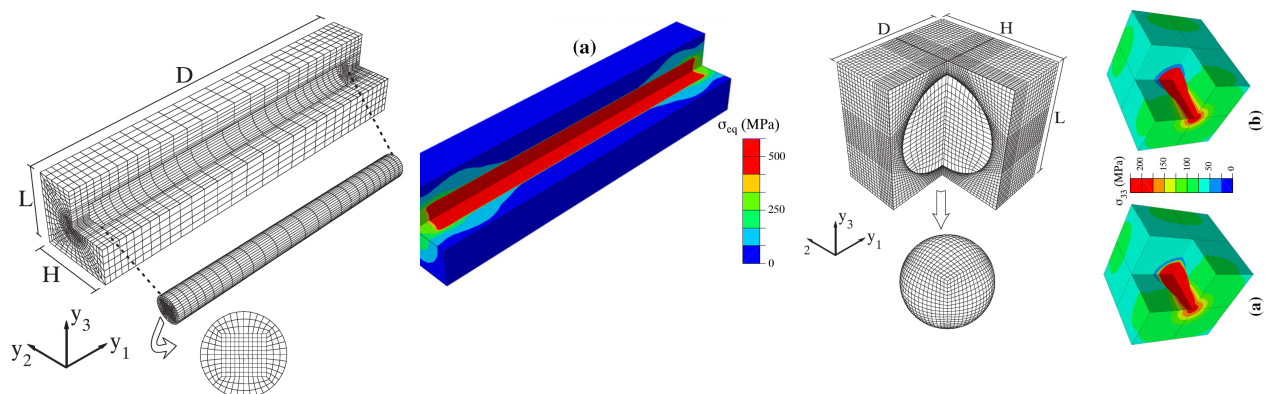


**Figure 26. Refined 3D parametric HFGMC repeating unit cells (RUCs) for two cases: Discontinuous long fiber and triply periodic medium with spherical inclusions.**

- 2) Ballistic impact of soft multi-layered composites with multi-scale meso-micro-models, Ref. [48] - This study deals with the mechanical properties of soft polymeric composite laminates made with Ultrahigh-molecular-weight polyethylene (UHMWP) fibers, used for ballistic protection. Two new mechanical test setups, tensile and axial shear, are proposed to characterize the mechanical behavior of a laminated system made of the commercial Dyneema® HB26 cross-ply multi-layered plates. A suitable tension setup is found to be close to a bow-tie like geometry while the axial shear is closer to a butterfly shape. Figure 27 shows the tension and shear testing setups along with Digital Image Correlation (DIC). The overall linear and nonlinear behaviors under both tension and shear are investigated. Explicit 3D finite-element (FE) dynamics is coupled with both meso-mechanical sublaminates models for repeated stack sequence through the thickness. Micromechanical GMC model is used for the individual layer as schematically shown in Figure 28.



**Figure 27. Left: Bow-tie specimen installed on the tension machine with extensometer; Right: Butterfly specimen assembled with pin holders. The top surface of the sample is randomly scattered with black and white small paint drops for DIC.**

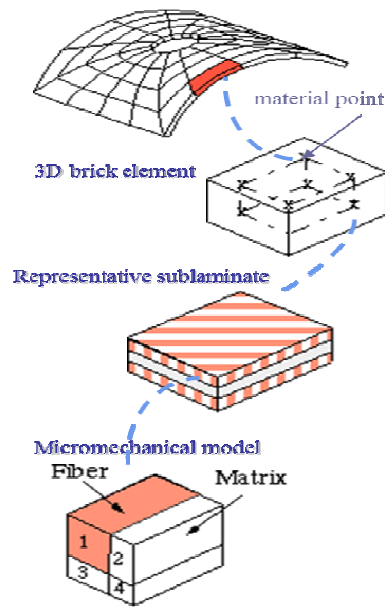


**Figure 28. Multi-scale 3D modeling of multi-layered composite**

Three major modes of failures are considered in the sublaminate meso-model. The first is a transverse out-of-plane shear which occurs typically at the entry of the projectile. The second and predominant model of failure is distributed delaminations between the layers. The third failure mode is fiber tearing which occurs at the end of the plate as the projectile attempts to exit and fully penetrate the plate. The static mechanical tests are used to calibrate a micro-mechanical model as a basis for the nonlinear stress-strain behavior while taking a factor to scale the static results and account for the high rate impact. Figure 29 Illustrate two cases with initial projectile velocities are 606 m/sec and 893 m/sec, respectively. The top row is high-speed test images while the bottom row is the predicted FE with multi-scale meso-micro-models at the same time frame of the experiment. The projectile penetrates the plate in the second higher speed case. Very good predictions are demonstrated by the proposed modeling framework.

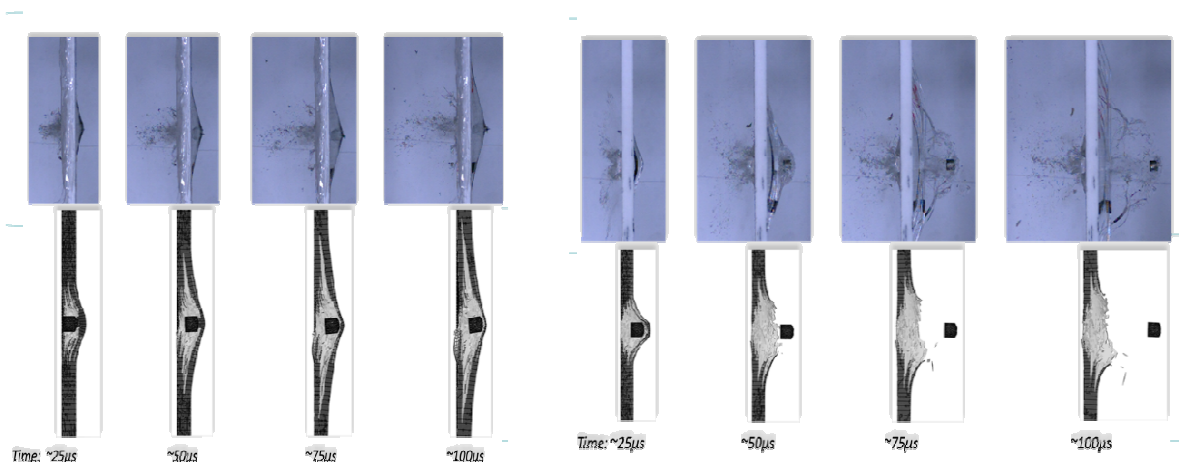


**Figure 29. Results from impact tests of two Dyneema® plates with steel projectile along with multi-scale damage simulations.**

## 4. PROBABILISTIC STUDIES

### 4.1 Probabilistic Crack Growth Behavior of Aluminum 2024-T351 Alloy Using the "Unified" Approach (G. Maymon, RAFAEL)

In the past, a deterministic experimental crack growth model for aluminum 2024-T351 alloy was formulated based on published experimental results, using the “unified” approach (Ref. [6]). In this research, random Equivalent Initial Flaw Size (EIFS) values obtained from other experimental results are introduced to the model, and the crack growth probabilistic behavior is demonstrated. The EIFS values computed from published experimental results of 3-D cracked fastener holes (Ref. [7]) are well-approximated by a Weibull distribution, as depicted in Figure 30. This approximated EIFS distribution is used as a distribution of the initial cracks in a large number of computations for a 2-D case which is very similar to the 3-D one, and serves for demonstration purposes. A computation program was then written to numerically solve the behavior of crack lengths vs. the number of load cycles.

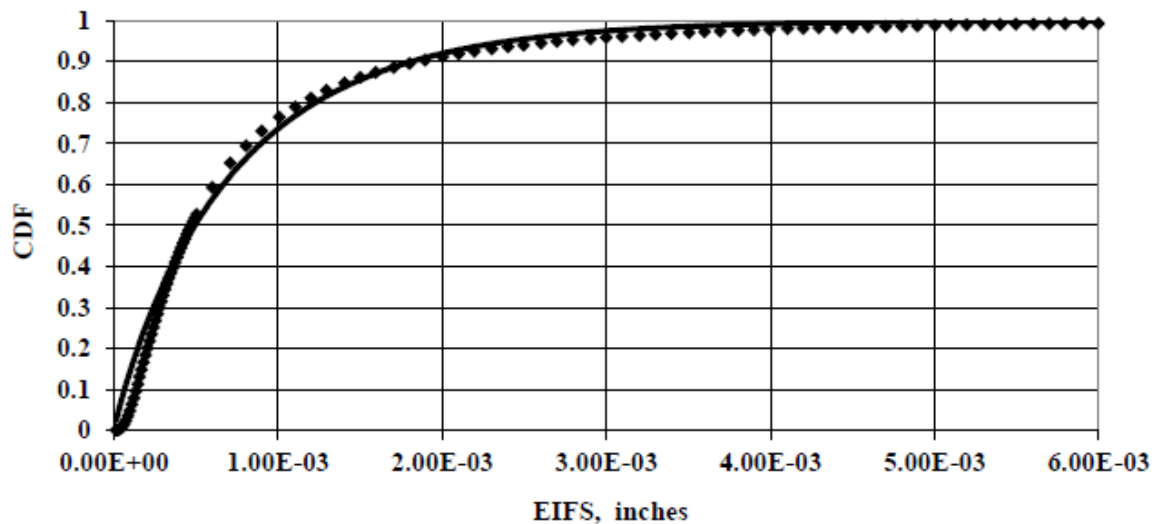


Figure 30. Cumulative distribution function (CDF) of test results versus approximated Weibull distribution

The probability of crack growth versus its initial crack length is obtained. It is shown that some of the cracks do not propagate upon cyclic loading, as their initial value is smaller than the required threshold criterion set by the “unified” approach. A dispersion in the number of load cycles required to obtain a given crack length is shown in Figure 31. Although the coefficient of variation (COV) of this dispersion is smaller than the COV of the initial random cracks, it may be of concern to designers, as the life period of the design may change by a factor of more than three.

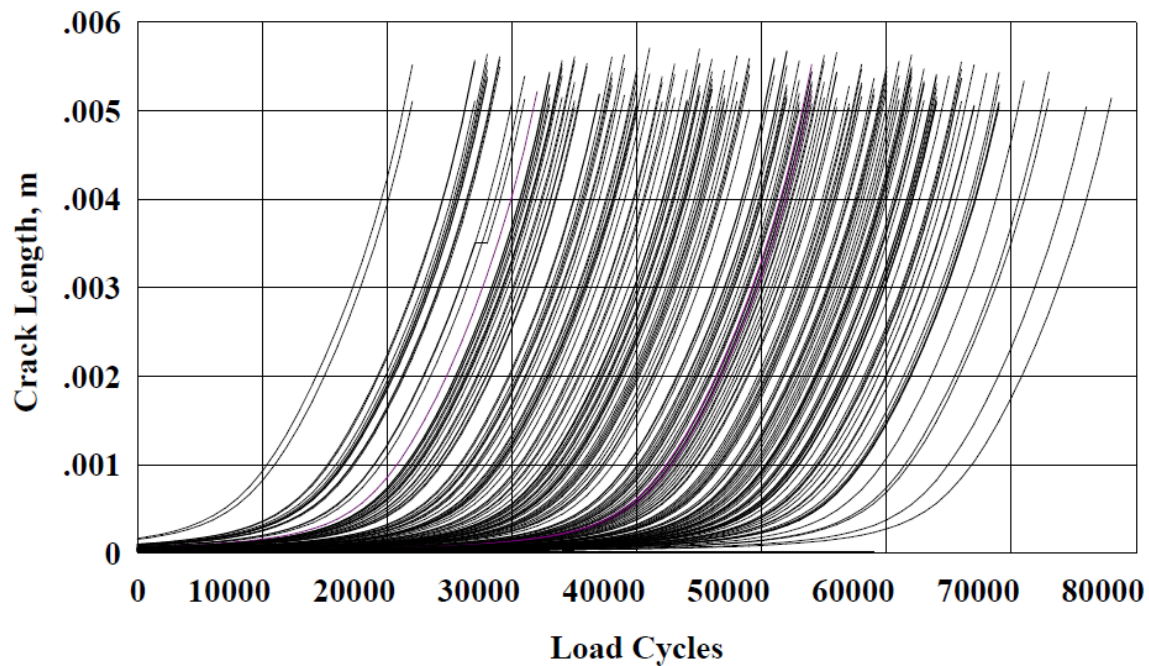
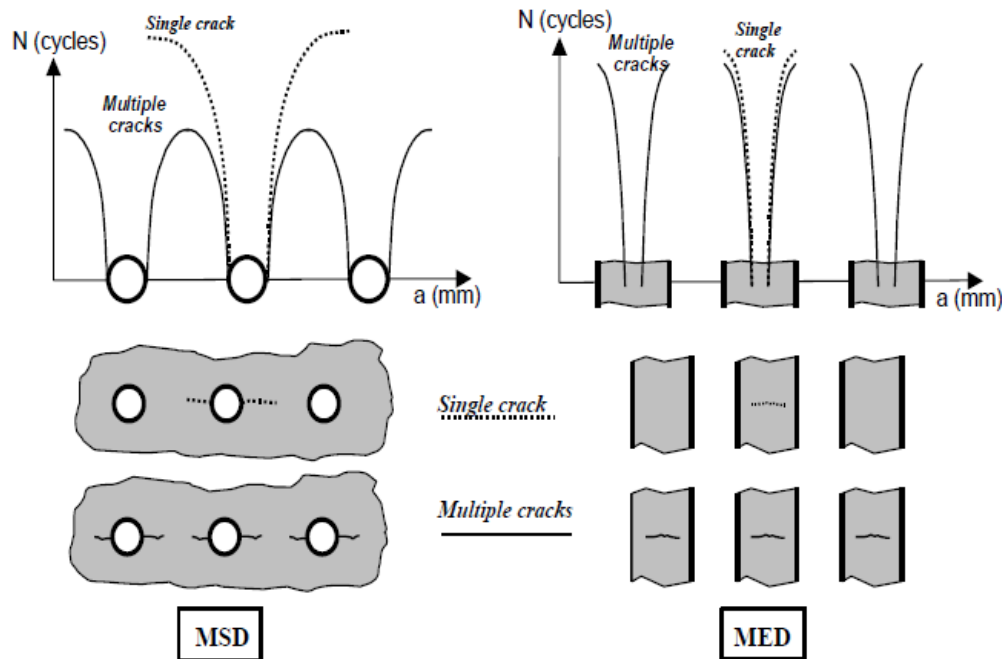


Figure 31. Crack growth curves of 500 samples (only 182 of them actually propagated)

A full length paper describing this investigation may be found in Ref. [8].

#### 4.2 A Risk Analysis Based Methodology for Widespread Fatigue Damage Evaluation (Y. Freed, D. Elmalich, A. Brot, Y. Buimovich, C. Matias, IAI)

*Widespread Fatigue Damage* (WFD) is the simultaneous presence of cracks at multiple structural locations that are of sufficient size and density such that the structure will no longer meet its required residual strength. It is common to divide the WFD phenomenon into two. A Multiple Site Damage (MSD) is a source of widespread fatigue damage characterized by the simultaneous presence of fatigue cracks in the same structural elements, whereas a Multiple Element Damage (MED) is a source of widespread fatigue damage characterized by the simultaneous presence of fatigue cracks in similar adjacent structural elements. Illustrations of MSD and MED are provided in Figure 32. Application of traditional damage tolerance analysis concepts is usually not sufficient to preclude WFD, since cracks related to WFD can grow quickly and interact in such a way that an operator cannot detect them in time before they lead to structural failure. A separate WFD assessment and determination of specific maintenance actions is necessary to adequately address WFD.



**Figure 32. Multiple Site Damage (MSD) and Multiple Element Damage (MED) interaction effects.**

The Widespread Fatigue Damage phenomenon was recognized by the aviation industry as one of the biggest threats on structural integrity, especially for ageing aircraft. The dramatic effect of WFD on aircraft structural integrity was demonstrated in April 1988 on Boeing 737 airplane operated by Aloha Airlines in Hawaii, when an 18-foot section of the aircraft fuselage flew off the airplane during flight. This accident drove the certification authorities to revise the relevant Federal Aviation Regulations paragraphs to ensure that the manufacturers account for the effect of WFD during the development and substantiation processes of transport category aircraft. During amendment 96 of FAR 25, paragraph 571(b) was revised to ensure, by "*sufficient full-scale fatigue test evident*", that the designer shows that WFD will not occur within the service goal of the airplane. Since WFD will happen to every airplane eventually, it was decided in 2011 to set a Limit Of Validity (LOV) of the engineering data that supports the structural maintenance program for each airplane. The LOV requirement is limited to large aircraft, in which its maximum takeoff weight is greater than 75,000 lbs. Once the LOV is established, airplanes must not fly beyond that point, unless additional engineering data are developed to support an extended LOV and any associated maintenance actions. This limitation ensures that WFD will not occur within the operational life of the aircraft.

Recently, a Notice of Proposed Amendment (NPA, Ref. [12]) of ageing aircraft structures was published by the European Aviation Safety Agency (EASA). This NPA, focusing on large aircraft, requires WFD assessment even for local repairs or alterations conducted on aging aircraft. This requirement is unique to the proposed EASA regulations, and is not included in the equivalent FAR 26 regulations, but it highlights the importance of the WFD assessment for aging aircraft.

Several approaches were suggested in the past for WFD assessment and to establish maintenance program, if applicable, to preclude WFD in fleet. All of them start by reviewing and identifying the structural elements which are suspected to WFD. The corresponding maintenance program is determined as follows. First, an average widespread fatigue lifetime  $WFD_{average}$  (i.e., lifetime in which widespread fatigue damage will initiate in 50% of the fleet) is obtained. This can be based on analysis supported by test evidence. Then an Inspection Starting Point (ISP) is defined. The ISP is the point in time when special inspections of the fleet are initiated due to specific probability of having an MSD/MED. The Structural Modification Point (SMP) is defined as well, as the point in time when a structural area must be modified to preclude WFD. Special inspection intervals are determined between the ISP and SMP.

Brot [13] presented a methodology to examine the admissibility of the inspection intervals in fatigue critical structures that is based on the risk analysis concept. In his analytical work, the inspection intervals for a typical lap-splice joint, which is prone to MSD, were determined using various NDI methods. The structure was then analyzed for the overall probability of failure (OPOF) using INSIM software [14].



In this study, a new approach to set the ISP, SMP and the corresponding inspection intervals is presented. Our approach is flexible in choosing ISP, SMP and inspection intervals, as long as the desired overall probability of failure is maintained. INSIM software is employed for the risk analysis evaluation (see Ref. [13] for more details). Based on our proposed approach, the operator can choose, for each structural detail which is prone to WFD, whether to adjust the inspection intervals, inspection threshold or the structural detail LOV, all while maintaining an equivalent probability of failure. Special attention is given to a lap-joint analysis, including validation to test results [15]. The full length paper will provide examples of lap joint WFD analyses as well as determination of various ISP, SMP and inspection intervals, all of which results in equivalent overall probability of failure to the lap joint structure.

This study will be presented at the 28<sup>th</sup> ICAF Symposium, 2015 [16].

## 5. STRUCTURAL HEALTH MONITORING

### 5.1 In-Flight, High Speed, Structural Health Monitoring System for High Altitude Long Endurance Unmanned Air vehicle (I. Kressel, J. Balter, IAI, N. Mashiach, O. Shapira, N.Y. Shemesh, B. Glam, A. Dvorjetski, IAF, I. Sovran, M. Tur, TAU)

This study presents the design, implementation, qualification and flight data evaluation of an in-flight Health and Usage Monitoring System (HUMS) embedded into the wings and booms of an Israeli Air Force High Altitude Long Endurance (HALE) Unmanned Aerial Vehicle.

Reliable flight data were recorded by the sensors during a dedicated flight test, covering the full UAV flight envelope, and continue to be recorded during the normal operation of the aircraft. The on-board collected data are processed off-line on the ground and analyzed both in the frequency and time domains so that critical components such as the individual UAV wing and booms load spectra and vibration signatures can be identified and tracked. The sensors data were also integrated with the flight parameters on a single GUI, Figure 33, for visual and quantitative correlation of the sensors readings and flight maneuvers. Based on the data obtained, it is now possible to track this UAV actual load spectrum and its impact on UAV structural integrity.

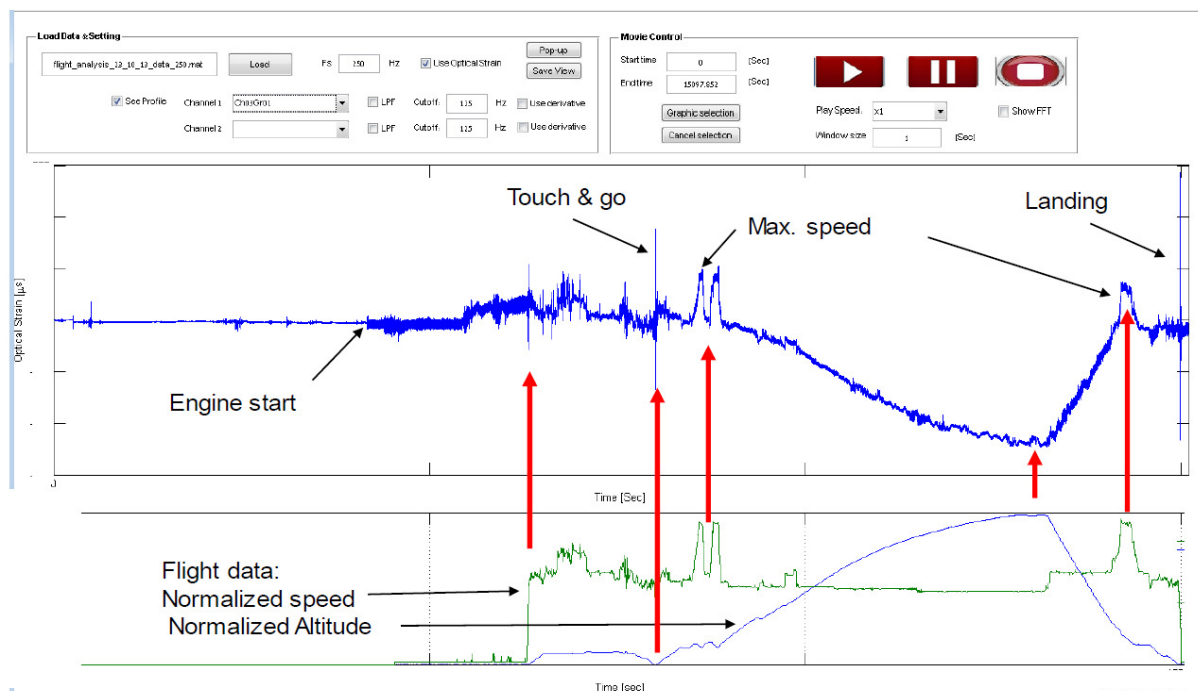


**Figure 33. Flight data GUI: Typical Boom FBG readings during flight : note the 'touch & go' maneuver and landing**

For accurate sensor placement at critical locations in the wing, a pre-fabricated glass-fiber composite sensing mat, containing the polyimide-coated optical fiber, was fabricated. This sensing mat was then bonded to the UAV structure, minimizing the risk of optical fiber damage and FBG sensor reflection attenuation. A solid-state, high sampling rate (2.5 kHz) FBG interrogation and data logger unit is used, capable of tracking multiple fibers, with multiple FBGs on each fiber. The interrogation unit was placed in the UAV payload bay and was powered by the UAV electrical system. Optical fibers were routed inside the UAV from the booms and wings to the interrogation unit.

The system was tested and calibrated on ground in order to verify its ability to track both static and dynamic boom and wing loading. Structural characteristics like strain distribution under static loading, impact response, and normal modes were successfully traced by the system. Since the UAV flies at different altitudes, where the temperature is significantly different than on ground, temperature compensation for the FBG data is required. On both booms and wing main spar, sensors are located in pairs: one on top, the other on the opposite bottom. Thus, each pair generates opposite strain readings with respect to bending loads. At the same time temperature induces approximately identical strains on both sensors. Assuming both the temperature and bending moment are the



same at each FBG pair location, the two unknowns, namely, the local temperature and mechanical strain can be derived once the temperature/strain to FBG wavelength deviations are properly ground calibrated. These two ground calibrations have been performed for the appropriate ranges of loads and temperature.

This fiber-optic-based sensing concept has already accumulated more than 1,000 flight hours without any failure. All major flight events were clearly detected by the FBG sensor net. The system is easy to operate and the visual GUI (Figure 33) enables a quick and basic evaluation of flight data, as well as providing a deeper analysis when required. Tracking the structural behavior over time can be used for Condition Based Maintenance (CBM), with the hope to eventually reduce maintenance cost and aircraft down-time.

## **5.2 Validation of a UAV composite wing spar repair using an embedded optical fiber Rayleigh back-scattering distributed strain sensing (A. Bergman, M. Tur, TAU, U. Ben-Simon, A. Schwartzberg, J. Burvin, I. Kressel, IAI, N.Y. Shemesh, B. Glam, IAF)**

This study reports a novel use of distributed fiber optic sensing to confirm and validate an innovative repair concept of a UAV primary structure.

A representing damaged UAV wing spar cap was repaired using bonded unidirectional composite materials. For such a repair concept, its strength and long-term durability depend on optimizing the geometry of the repair in order to minimize stress concentration in the adhesive. In order to assess the stress distribution along the repair bond-line, an optical fiber was embedded during the repair application for distributed Rayleigh back-scattering strain measurement. The fiber was placed inside the structure, therefore enabling taking strain measurements, at a high spatial resolution, under the wing skin directly on the repair. This type of distributed sensing is an excellent alternative to the conventional electrical strain gauges that are discrete and can only be placed on the outer surface where the adhesive stress concentration is masked by the skin and can be missed.

The Rayleigh 'signature' of the fiber is recorded at a reference state and then when the fiber is strained, the modified new reading is correlated with the reference to produce a measure of the strain/temperature change the fiber had experienced. This is a high resolution technique (~1cm), requiring no preparation on the part of the fiber.

Three specimens were tested statically and under fatigue spectrum, all monitored by means of embedded optical fibers. The first two specimens, tested up to failure, were used to optimize the repair concept and the third one was a full scale wing spar portion representing the actual repaired spar and the leading edge. This last specimen was tested up to ultimate load followed by cyclic loading spectra representing several lifetimes of the structure. During this entire test, strain measurements were taken periodically.

The repair concepts and their strain measurements, taken during the 1<sup>st</sup> and 2<sup>nd</sup> ultimate tests are shown in Figure 34. It is clearly seen that the observed dependence of strain to load is highly nonlinear for stepped joint repair. This nonlinearity corresponds to sharp changes in the repair stiffness, stressing the adhesive beyond its linear limit at two locations in the repair. For the second specimen, where the repair concept was designed to avoid stress concentration, it is seen that the stress concentration at the joint critical location is very small and no nonlinearity is observed.

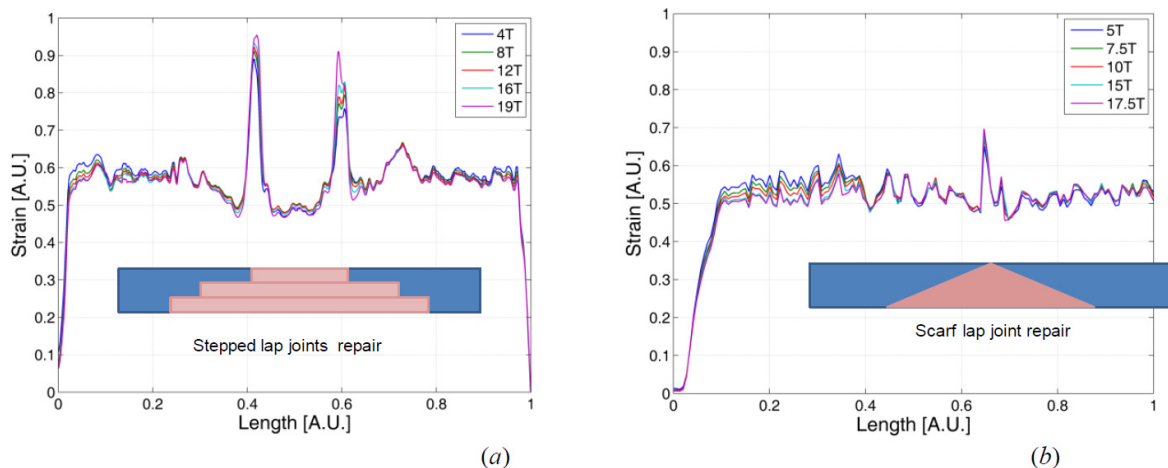


**Figure 34. Normalized strain distribution in the repair specimens; (a) First specimen: stepped lap joints repair concept; (b) second specimen: scarf repair with gradual stiffness change.**

As a result of this adhesive overstressing, the stepped lap joints specimen with sharp stiffness change failed at approximately 66% of the ultimate failure load of the second scarf repair specimen. Based on these results, the 3rd specimen, a 6 meter long UAV wing spar repaired by the scarf lap concept, was successfully tested statically up to the ultimate design load followed by fatigue and residual limit loading. It was demonstrated that the repair strain distribution remains the same during the entire duration of the test, verifying that the repair airworthiness is maintained.

This study will be presented at the 28<sup>th</sup> ICAF Symposium, 2015 [54].

### 5.3 Progress at BGU HUMS Laboratory (J. Bortman, BGU)

In recent years, Ben Gurion University (BGU) Health and Usage Monitoring Systems (HUMS) Laboratory focuses on application of vibrations and acoustical measurements for early detection of damages in mechanical components. Vibration monitoring can be used to detect machine faults, including: unbalance, misalignment, oil film bearing instabilities, roller bearing degradation, gear damages, mechanical looseness, structural resonance, and cracked rotors. It is applicable to a range of industrial machines such as energy turbines, engines, helicopters, ships or land vehicles.

An example of such research is provided in Ref. [20], in which a new 3D dynamic model for ball bearings with and without faults was introduced. This model is based upon the classic dynamic and kinematic equations, Hertz type contact force and hyperbolic-tangent friction model. The motion equations are incrementally solved, assuming constant acceleration for each time step. The model was validated by comparing its results to a known analytical solution of a "healthy" bearing and a well-established acceleration signal pattern of a locally faulted bearing. It is further verified by showing the numerical convergence of the vibration signature and by its forward comparison to empirical test results. In [21], it is assumed that the spall generation on the surface of a raceway is a result of Rolling Contact Friction (RCF). RCF occurs when two bodies roll/slide with respect to each other, producing alternating stresses over a very small volume beneath the contact surface (see Figure 35 for more details). Complete understanding of the fatigue process is critical for estimation of the bearing remaining useful life and allows planning maintenance actions. This process is modeled based on continuum damage mechanics and later implemented using ABAQUS Finite Element software. Different meshes were constructed for simulation purposes. An ideal line contact, representing the cylindrical roller bearing, is used to simulate rolling contact conditions. The geometry and initiation time of the simulated spalls were found to be in good agreement with published simulated and experimental data. An example of the spall patterns for different simulations is provided in Figure 36.

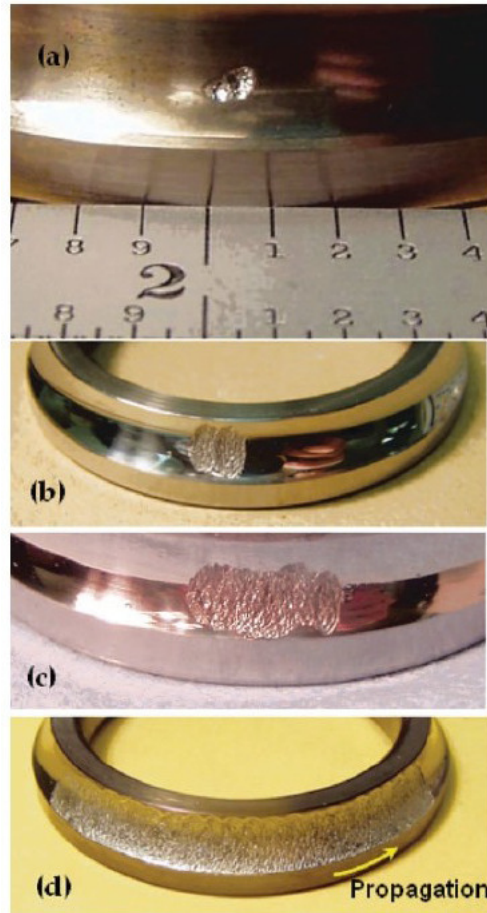


**Figure 35. Fatigue spall initiation on inner raceway; (b), (c), and (d) show progressive propagation of the initiated spall under RCF [21].**

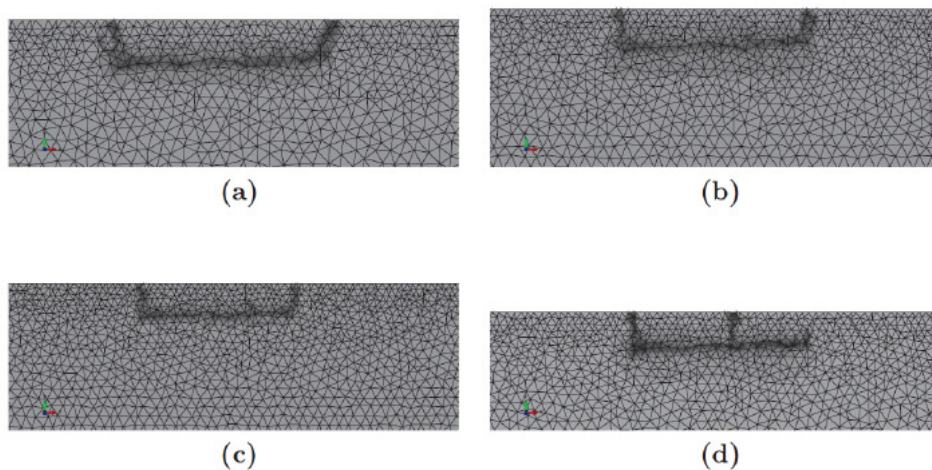


**Figure 36. Spall pattern of four different simulations.**

The effect of fault size on the bearing dynamics was investigated in [22]. The research methodology combines dynamic modeling of the faulty bearing with experimental validation and confirmation of model simulations. In this study, small faults (starting from 0.3 mm), simulating incipient damage, are generated at increasing sizes by an electrical discharge machine. The recorded vibration data is then analyzed and compared to the vibration signatures predicted by the model. It was found that the behaviors of the acceleration RMS levels as a function of the fault size are similar in the experimental and the predicted results. In both cases, the general RMS level increases. In addition, a new insight was found about the relation between the vertical and the horizontal vibration levels as function of fault size and fault location. It was concluded that the model provides a good prediction about trends and pattern of localized faults.

Next, the identification of possible faults in gear wheel systems is investigated in [23]. To date, the majority of existing condition indicators for gears are based on various statistical moments of a recorded time history. In this study, a combined analytical and empirical approach is applied. This approach is based on the assumption that reliable dynamic models can be utilized to predict the effects of faults on vibrational patterns. Dynamic model generated signatures are used to verify experimental findings. Moreover, discrepancies between simulated and actual results, combined with understanding of the assumptions and omissions of the model, are helpful in understanding and explaining the experimental results.

A spur gear transmission setup was used for experiments, along with an electric AC motor and a friction belt loading device. The experimental runs were conducted at varying speed settings. Two types of faults, a tooth face fault and a tooth root fault, were seeded in the experimental transmission and into the model. The effect on extracted signal features was examined. An example of PSD output for healthy versus damages gear wheel is provided in Figure 37.

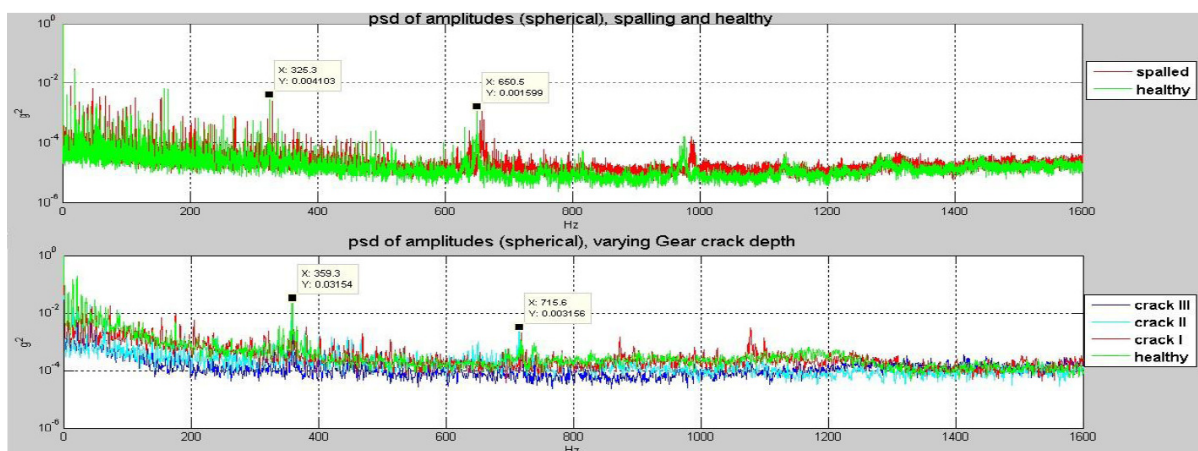


**Figure 37. PSD (spherical) of frequency domain, (a) spall vs. healthy, (b) various degrees of cracked gear.**

## 6. MISCELLANEOUS

### 6.1 Time Reversal for Crack Identification (E. Amitt, D. Givoli, E. Turkel, Technion)

This study propose a general computational methodology for identifying cracks in structures. It is based on a time reversal technique and on the notion of refocusing. In the proposed procedure, a known source generates waves in the structure, and the time-varying response of the structure is measured only at certain points and times. In an industrial application, this step is performed experimentally, but in the present study it is emulated numerically. Relying on a computational model of the structure and on the measured signals, a TR solution is obtained for each assumed set of crack parameters. This amounts to evolving the solution backward in time, till the initiation time of the original source. The crack identification is based on seeking, among all crack candidates, the crack which yields the best wave refocusing at the true source location. To test the proposed methodology, a simple rectangular membrane model governed by the 2D time-dependent scalar wave equation is employed. Finite element discretization of the structure and an explicit time-stepping scheme are used. The performance of the method is tested under various conditions and with various amounts of partial information. Its sensitivity to noise and to perturbations in the material properties is also investigated.

Figure 38 presents time reversal solutions for three different candidate cracks. More details on this procedure are provided in Ref. [2944].

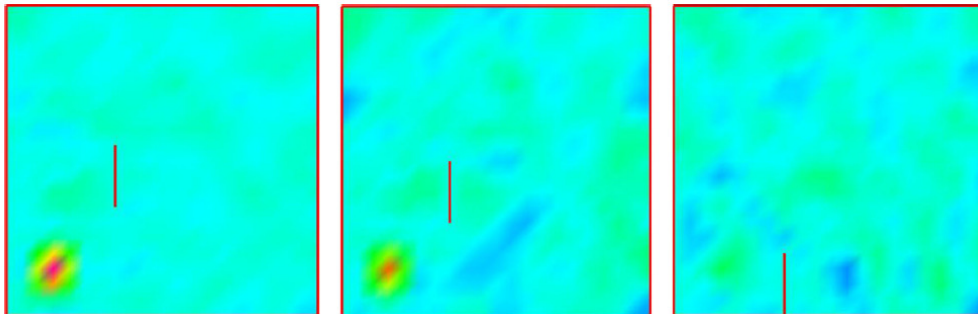


Figure 38. Time reversal solutions obtained for three candidate cracks.

### 6.2 TaxiBot - A New Concept for Towing Airplanes with Engines Stopped (R. Braier, IAI)

Since the start of the widespread use of towbarless towing, there have been many attempts to tow aircraft directly from the gate to the takeoff runway (dispatch /operational towing) with Engines Stopped, this in order to save fuel and reduce noxious gases and noise pollution. In the past, these proposals have all been dismissed by the airframe manufacturers due to the expected reduction of the fatigue life of the Nose Landing Gear, due to the many towing load cycles that will be applied during dispatch towing.

Nevertheless, the dispatch towing concept has many advantages. A study has shown that an annual savings of \$5.3 billion of fuel expenses and 20 million tons of CO<sub>2</sub> emission can be realized, if all Wide-Body and Narrow-Body aircraft are towed to their takeoff points (*a large 4 engines wide-body aircraft burns about 355 gallons of fuel for every 17 minutes of taxi-out time needed to reach its takeoff point*).

IAI, together with TLD and other subcontractors with the support and Airbus and Boeing, has developed a semi-robotic towbarless towing vehicle called TaxiBot (Taxiing Robot). Under this concept, the pilot of the aircraft remains in full command during the entire towing process, in contrast with the regular dispatch towing where the driver is in control. In order to slow down and /or stop, the pilot is applying the aircraft brakes (at the Main Landing Gears) as needed, as opposed to regular dispatch towing where the tractor is stopping the convoy. By slowing / stopping the convoy by the airplane, the magnitude of the load applied on the Nose Gear is reduced significantly, by the airplane-to-tug mass ratio (10 for wide-body airplanes and 3-5 for narrow-body). This mass ratio and the fact that the bigger mass is stopped by the aircraft brakes is reducing 66%-90% of the physical loads applied to the Nose Landing Gear during the convoy slowdown and braking. The airplane engines will be started-up only shortly before takeoff.

This concept has been proved during a TaxiBot Demonstrator testing, see Figure 39. Test measurements have confirmed that TaxiBot towing will not result in any reduction of the Nose Landing Gear fatigue life.



**Figure 39. Airbus A340-600 and Boeing B747-400 towed by TaxiBot**

The next step was to build a Prototype to tow Narrow Body (NB) airplanes, to integrate, test and certify. The French company TLD, the biggest GSE manufacturer, produced the TaxiBot NB prototype basic vehicle which was tested during one and a half years in Chateauroux airfield in France.

The program acquired a grounded A320-200 airplane and instrumented it to serve as real condition test bed, see Figure 40. At June 2013 the first pre-serial production TaxiBot NB the PRS1 was delivered to Frankfurt airport for adaptation and testing with a B737-500 test airplane, provided by Lufthansa. Till the end of March 2014 the following PRS2 and PRS3 were delivered to Frankfurt to support the certification tests campaign.



**Figure 40. TaxiBot NB prototype towing the Airbus A320-200**

The B737-500 is the most challenging platform in the Narrow Body commercial aircraft manufactured by Boeing and Airbus, since the mass ratio between the aircraft and the vehicle is 2 (A/C MTOW 54 tons and vehicle weight 26.5 tons). In addition, the loads on the NLG of this airplane are the highest in the B737 family and the A/C wheel base is the shortest in the family. The lowest mass ratio, the shortest wheel base and the highest NLG loads on the B737-500 are the most extreme case and the most challenging for the TaxiBot control system in terms of controlling the loads on NLG, since the weight of the vehicle comparing to the A/C weight is more than 50%. The short wheel base is also the most challenging case from the steering stand point; since the A/C maneuverability is greater than all other airplanes (A/C maneuverability is greater as much as the wheel base is smaller). High maneuverability generates high sensitivity to pilots steering inputs, which become over sensitive above 15 knots. We had to develop a special algorithm to adapt the TaxiBot reaction to pilot steering inputs in order to give the pilot a "transparent feeling" at all speed ranges from 1 knots to 22-23 knots.

Following the final adaptation for the B737-500 the certification test have started in Frankfurt with EASA and CAAI certification authorities. The certification test included 132 test of all emergency cases and malfunction on the system as well as careful testing and measurements of the TaxiBot ability to maintain the designed fatigue envelop defined by IAI experts with the support of Boeing (Figure 41). Keeping the fatigue envelop in real time

under all normal taxiing condition and the static envelop in all emergency cases were the main focus of the authorities, that participated and witnessed the testing, via a real time display of the loads measured during the tests. Finally in October 2014 the TaxiBot have granted the Supplement Type Certificate (STC) for the B737 classic family. Following the certification document issued by EASA the TaxiBot PRS vehicles have started the In Service Evaluation phase in Frankfurt with commercial flights. The First commercial flight that was dispatched with passengers from Frankfurt was flight LH130 on November 25, 2014.



**Figure 41. TaxiBot NB, PRS1 in operation at Frankfurt international airport**

TaxiBot wide body (WB) prototype have finished its assembly by the end of last year and started integration and dynamic tests at the new TLD factory in Sorigny France (near Tour). In April the WB TaxiBot is expected to start testing with the test trailer that simulates a B747 airplane (with B747 cockpit and NLG) in Sorigny and later in Chateauroux airport. Later in November we will start the test with a Lufthansa B747-400 airplane and prepare the system for its certification tests at the first half of 2015.

Summary:

- **TaxiBot is the Only Certified and Operational system for taxiing airplanes to takeoff with engines stopped**
- TaxiBot program is an excellent encounter between economical & environmental interests worldwide :
- Compatible to 100 seats or more (Boeing and Airbus)
- Maintain the pilot's responsibility (while being transparent)
- Working closely with airlines, airports
- Most studies on main Hub airports showed – No need for infrastructure changes in order to implement TaxiBot operation
- No modification to airplane system – plug and play for all NB and WB airplanes
- No additional weight to any airplane
- No reduction in airplanes Cargo Space due to TaxiBot operation
- Transparent system to pilot operation as per pilots feedback from tests – No need for pilots practical training
- The only solution that will remain available for years on most current and future aircraft fleets for any flight range

### **6.3 Progress at the Dreszer Fracture Mechanics Laboratory (L. Banks-Sills, TAU)**

During the last two years, characterization of the behavior of delaminations between layers of fiber reinforced, laminate composite material has been continuing. A Ph.D. student completed a Ph.D. thesis on determining the nearly mode I interface fracture toughness  $G_{ic}$  and fatigue behavior of a multi-directional woven composite made of a carbon/epoxy composite prepreg G814/913 (Ref. [34]). Note that the subscript  $i$  represents interface. A double cantilever beam (DCB) specimen was used for the tests as shown in Figure 42 . The specimen was comprised of 15 layers alternating between a  $0^\circ/90^\circ$  weave and a  $+45^\circ/-45^\circ$  weave. Analysis of the tests showed a

slowly rising  $G_R$ -curve (see Figure 43). The bar over the energy release rate  $G$  represents the average value through the thickness.

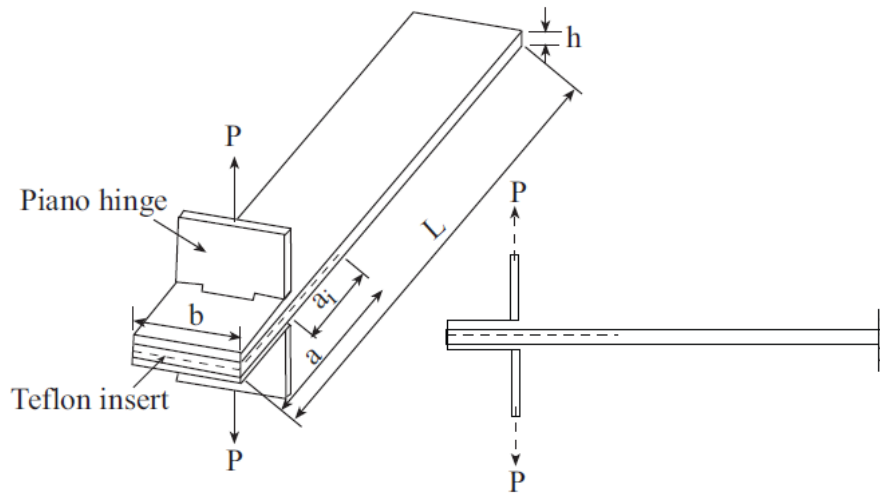


Figure 42. Double cantilever beam woven composite specimen.

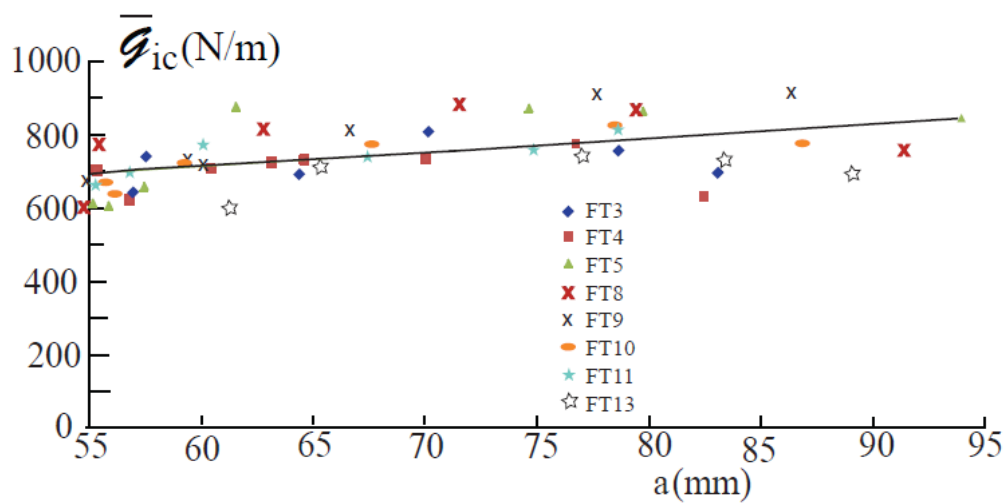
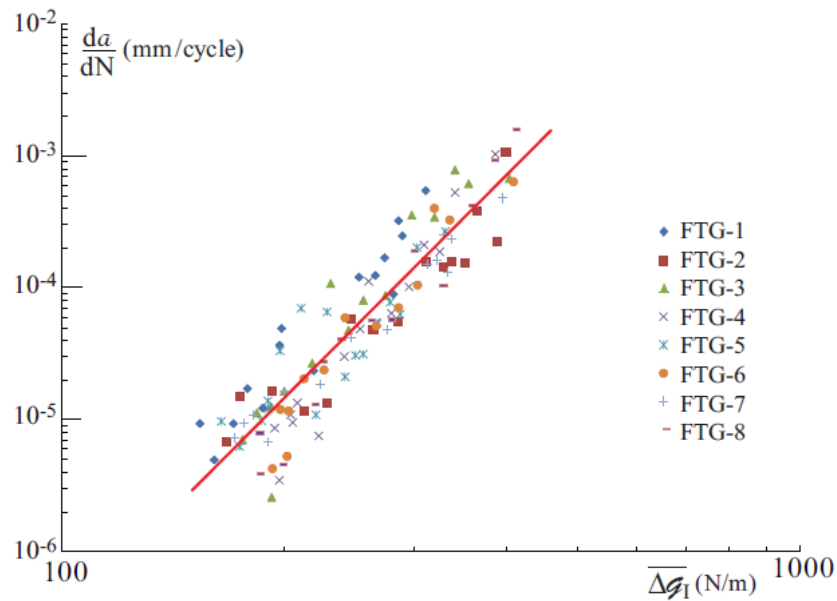


Figure 43. Average critical interface energy release rate  $G_{ic}$  as a function of delamination length

The relation between  $G_{ic}$  and the increase in crack length  $\Delta a = a_0 - a_i$  where  $a_0$  is the initial crack length and  $a_i$  is the current crack length was found to be

$$G_R = 670 + 580(\Delta a)^{0.4} \quad (1)$$

A paper on this subject was published in the International Journal of Fracture (Ref. [35]).



**Figure 44. Delamination growth rate  $da/dN$  vs.  $\Delta G_I$ .**

In addition, the fatigue delamination behavior of this interface consisting of the same composite material was studied. Eight fatigue tests were carried out to determine the delamination growth rate  $da/dN$  vs. the nearly mode I cyclic energy release rate  $\Delta G_I$ . The tests were carried out by means of displacement control. A constant cyclic displacement ratio  $R_\delta = \delta_{\min}/\delta_{\max} = 0.1$  was used in the tests. The results are presented in Figure 44. The fitted line is given by

$$da/dN = 1.77 \times 10^{-18} (\Delta G_I)^{5.61} \quad (2)$$

Comparison of the delamination growth rate was made to the crack propagation rate of an aluminum alloy. It was found that a crack in the aluminum will grow faster but will be less sensitive to uncertainties or changes in load level. A paper was published in Composites Part B (Ref. [36]). Different parts of this work were presented at the Engineering Structural Integrity Assessment Meeting in Manchester, UK (Ref. [37]) and International Conference on Experimental Mechanics in Cambridge, UK (Ref. [38]). This work is being continued by an M.Sc. student who is considering the effect of block loading on the fatigue propagation of the delamination in this material.

The high power in eq. (2) makes the equation difficult to use for a damage tolerance approach to fatigue delamination propagation. A new approach is being applied to reduce the slope of the  $da/dN$  vs.  $\Delta G_I$  equation. In addition, mixed mode tests for this interface are planned using the Brazilian disk specimen. Further work is being carried out on a wet lay-up with a delamination between a unidirectional upper ply with fibers in the  $90^\circ$ -direction and a  $0^\circ/90^\circ$  woven lower ply. The Brazilian disk specimen is being used to determine the mixed mode fracture toughness of this composite. Some tests have been carried out and analyzed. These tests are continuing and will be reported on in the next national review.

A review paper has been published on the topic of interface fracture and delamination failure of composites in Strain (Ref. [39]). In addition to the review of the subject, new ground was broken in proposing a failure criterion with an assigned probability. In that study, the  $t$ -statistic was used to guarantee a failure probability of no more than 5%. Parts of these topics have been presented at the University of Peking in Beijing (Ref. [40]), the European Conference of Fracture in Trondheim, Norway (Ref. [41]) and the Seventh International Conference on Fracture of Polymers, Composites and Adhesives in Les Diablerets, Switzerland (Ref. [42]).

Another area of interest has been the effect of reinforcement of a polymer with low weight fractions of carbon nanotubes (CNTs). Three students have worked on this project. Or Ben David completed an M.Sc. degree on the characterization of mechanical properties of poly methyl methacrylate (PMMA) reinforced with CNTs (Ref. [43]). Tal Simhi completed an M.Sc. degree on the determination of mechanical and fracture properties of PMMA reinforced with CNTs (Ref. [44]). As a result, a paper was published on this subject in Experimental

Mechanics (Ref. [45]). Finally, another student, Guy Shiber, is working towards an M.Sc. degree on mechanical properties of PMMA enhanced by functionalized CNTs.

The effective mechanical properties of PMMA reinforced with CNTs were evaluated by means of two approaches: experiments and a micromechanical model (Ref. [45]). With various concentrations of CNTs, two specimen fabrication processes were examined: hot pressing (HP) and injection molding (IM). Experiments included a series of uniaxial tensile tests guided by an ASTM standard. Using displacement control, tests were carried out while images were taken of the gage area. The in-plane displacement fields were evaluated by means of Digital Image Correlation (DIC). A MATLAB program was then used to calculate strains, create stress-strain and strain-force curves and determine Young's modulus  $E$ , Poisson's ratio  $\nu$ , the ultimate tensile stress  $\sigma_{\text{uts}}$  and the strain to failure  $\varepsilon_f$ . In addition, simulations were carried out using a micromechanical model (High-Fidelity Generalized Method of Cells or HFGMC). A Repeating Unit Cell (RUC) consisting of one CNT and PMMA surrounding it was modeled and analyzed in order to determine the effective mechanical properties of the composite. This method allows for imperfect bonding between the phases which is controlled by two parameters. These damage parameters decrease the stress-strain response of the material. However, the increase of the volume fraction increases the composite response. These two conflicting effects appear to provide the observed decrease in Young's modulus for low volume fractions as discussed. The effects of CNT concentration, geometry and orientation, as well as the interface between the phases, were examined. It was seen from the experimental results, for HP specimens and low concentrations of CNTs,  $E$  initially decreases and then increases significantly as the weight fraction increases. This behavior of  $E$  was quantitatively predicted by the HFGMC model. For IM specimens, Young's modulus is nearly constant for low weight fractions of CNTs and then increases with weight fraction. Parts of this work were presented at the 16th Composite Materials Symposium in Haifa, Israel (Ref. [46]). A further study is being carried out on functionalized CNTs. That is, their surface has been treated so that a stronger interface between the CNTs and polymer should be attained.

The influence of CNT concentration on the fracture toughness of PMMA was examined on single edge notched beam IM specimens. Six groups of specimens containing 0.5, 1, 2, 4, 8.5 wt% of CNTs and neat PMMA as a reference were tested. First, a notch was introduced into the specimens by a specially made disk whose edge is V-shaped with a  $30^\circ$  angle and a  $30 \mu\text{m}$  tip width. As suggested by an ASTM standard for polymers, induction of a natural crack was attempted, without success. Therefore, fracture toughness values were determined with the sharp notch by means of a calibration formula for a natural crack. These were compared to values obtained using a stress concentration factor and found to differ by less than 3%. The latter calculation takes into account the geometry of the notch. Results showed a decrease in the fracture toughness values with an increase in the CNT concentration. For the natural crack, a significant increase in fracture toughness was observed, as a result of the induced damage.

#### 6.4 Progress at BGU Computational Mechanics Laboratory (Z. Yosibash, BGU)

Singularities associated with three dimensional domains, especially in the vicinity of V-notch tips crack fronts have been investigated in our group during the past two years. A newly developed method, named the quasi-dual function method (QDFM) was proposed for extracting edge stress intensity functions (ESIFs) along circular crack fronts from finite element solutions, in a general three-dimensional domain and boundary conditions. The mathematical machinery was applied for the extraction of ESIFs from high-order finite element solutions in [30]. The QDFM has several important advantages:

- It allows to extract the ESIFs away from the singular edge, thus avoiding the need for a refined FE mesh
- The ESIFs are obtained as a function along the edge and not as pointwise values
- The method is general in the sense that it is applicable to any circular edge (be it a penny shaped crack, a cylindrical crack or a circular external crack).

Numerical examples that demonstrate the efficiency, robustness and high accuracy of the proposed QDFM were provided.

The study on curved singular edges was extended to elliptical cracks in Ref. [31]. Since explicit asymptotic solutions are unavailable for elliptical crack or sharp V-notch in a three-dimensional elastic domain, the Laplace equation was first considered for their derivation. Both homogeneous Dirichlet and Neumann boundary conditions on the surfaces intersecting at the elliptical edge were considered. For the first time these asymptotic solutions were derived in an explicit form and demonstrated, just as for the circular edge case, that these are composed of three series with eigenfunctions and shadows depending on two coordinates.



The computation of the edge flux intensity functions associated with the integer eigenvalues (for the Laplace equation) was also addressed by the QDFM in three dimensional domains [32]. The first integer eigenvalue is associated with the T-stress in the theory of elasticity. For the integer eigenvalues it was shown that the dual eigenpairs and shadows, exhibit the presence of logarithmic terms in the dual singularities. These were then used with the QDFM to extract EFIFs from p-version finite element solutions.

Criteria that may predict crack initiation location and instance in 3D brittle elastic materials containing sharp V-notches under a complex stress state are unavailable. Towards the development of such criteria based on the combination of the stress criterion on one hand and the energy release rate criterion on the other hand one needs the difference in the potential energy in an elastic three-dimensional domain with a V-notch with and without a small crack under a general mixed mode I+II+III loading. This is provided as an asymptotic series in [33]. It involves the V-notch edge stress intensity functions, the area of the formed crack, and special geometrical functions that can be pre-computed and tabulated. Importantly, the stress intensity functions along the crack front and the solution for the V-notched domain with the presence of the crack are un-necessary. The analytical formulation was verified by finite element methods, demonstrating the accuracy of the obtained expressions.

## 7. REFERENCES

1. Brot, A. and Freed Y., "Review of Aeronautical Fatigue Investigations in Israel, April 2011 – March 2013", *Minutes of the 33rd ICAF Conference*, Jerusalem, Israel, 2013.
2. Brot A. and Matias C., "The effects of Residual Tensile Stresses Induced By Cold-working a Fastener Hole", *USAF Structural Integrity Program (ASIP) Conference*, 2007.
3. Brot A and Matias C., "Residual Tensile Stresses Induced by Cold-Working a Nearby Fastener Hole", *Proceedings of the 47th Israel Annual Conference on Aerospace Sciences*, 2007.
4. Freed Y., Dolev O. and Amran Y., "Investigation of Crack Nucleation in the Vicinity of Cold-Worked Fastener Holes", *Proceedings of the 54th Israel Annual Conference on Aerospace Sciences*, 2014.
5. Nakada, M. and Miyano., L., "Accelerated Testing for Long-Term Fatigue Strength of various FRP Laminates for Marine use", *Composites Science and Technology* 69 (2009), p. 805-813.
6. Maymon G., "A "unified" and a  $(\Delta K^+ \cdot K_{\max})^{1/2}$  Crack Growth Models for Aluminum 2024-T351", *International Journal of Fatigue* 27 (2005), p. 629-638.
7. Norohna P.J. et al., "Fastener Hole Quality", Vol. I, AFFDL-TR-78-206, Wright Patterson AFB, 1978.
8. Maymon G. "Probabilistic Crack Growth Behavior of Aluminum 2024-T351 Alloy Using the "Unified" Approach, *Proceedings of the 54th Israel Annual Conference on Aerospace Sciences*, 2014.
9. Diamant, G. and Buimovich, Y., "Automated Gust Loads Spectrum for Fatigue Analyses of Aircraft", *Proceedings of the 54th Israel Annual Conference on Aerospace Sciences*, 2014.
10. Zur, C., Buimovich Y., Freed, Y. and Ramati, S., "Examination of the Influence of Flap Peening Process on the Fatigue Life of Straightened Metal Elements", *Proceedings of the 55th Israel Annual Conference on Aerospace Sciences*, 2015.
11. Brot, A., "Modernization of the S-N Diagram for Fatigue Life Analysis", *Proceedings of the 54th Israel Annual Conference on Aerospace Sciences*, 2014.
12. Ageing Aircraft Structures, Notice of Proposed Amendment 2013-07, 23.4.2013.
13. A. Brot, "Optimizing the Inspection Intervals for Aircraft Structures Prone to Multi-Site Damage", 53rd Israel Annual Conference on Aerospace Sciences, 2013.
14. INSIM, INspection SIMulation software, ver. 3.0.
15. H. Vlieger and H.H. Ottens, "Uniaxial and Biaxial Tests on Riveted Fuselage Lap Joint Specimens", Report No. DOT/FAA/AR-98/33, 1998.
16. Y. Freed, D. Elmalich, A. Brot, Y. Buimovich, C. Matias, "A Risk Analysis Based Methodology for Widespread Fatigue Damage Evaluation", *Proceedings of the 28<sup>th</sup> ICAF Symposium*, 2015.
17. J. Kunz and J. Siegl, "Fractographic Marking of Fatigue Fracture of Aircraft Structure Parts", V-KMAT-625/05.
18. NASGRO - Fracture Mechanics and Fatigue Crack Growth Analysis Software; Version 7.1, 2014.
19. C. Matias, A. Brot, G. Noivirt, C. Zur and Y. Amran, "Mutual Influence of Two Opposite Cracks at a Hole", *Proceedings of the 55th Israel Annual Conference on Aerospace Sciences*, 2015.
20. G. Kogan, R. Klein, A. Kushnirsky and J. Bortman, "Toward a 3D dynamic model of a faulty duplex ball bearing", *Mechanical Systems and Signal Processing*, DOI: 10.1016/j.ymssp.2014.07.020.

21. D. Gazizulin et al., "Towards a Physics Based Prognostic Model for Bearing – Spall Initiation and Propagation", *IEEE Aerospace Conference*, Montana, USA, 2015.
22. M. Mendelovich, Y. Sanders, G. Kogan, M., R. Klein and J. Bortman, "Characterization of Fault Size in Bearings", *Annual Conference of the Prognostics and Health Management Society*, 2014.
23. A. Bliznyuk, I. Dadon, R. Klein and J. Bortman, "Gear Diagnostics – Fault Type Characteristics", *Annual Conference of the Prognostics and Health Management Society*, 2014.
24. M. Perl, and J. Perry, "The Beneficial Influence of Bauschinger Effect Mitigation on the Barrel's Safe Maximum Pressure", *Trans. of the ASME, Journal of Pressure Vessel Technology* 135, (2013).
25. Q. Ma, C. Levy and M. Perl, "A Study of the Combined Effects of Erosions, Cracks and Partial Autofrettage on the Fatigue Life of a Thick Walled Pressurized Cylinder," *Trans. of the ASME, Journal of Pressure Vessel Technology* 135 (2013).
26. M. Perl, M. Steiner and J. Perry, "3-D Stress Intensity Factors due to Autofrettage for an Inner Radial Lunular or Crescentic Crack in a Spherical Pressure Vessel, accepted for publication in *Engineering Fracture Mechanics*.
27. Q. Ma, C. Levy and M. Perl, "The Bauschinger Effect's Influence on the SIFs of a Semi-Elliptical Crack Emanating from an Erosion at the Bore of a Fully Autofrettaged Pressurized Cylinder," accepted for publication in *Trans. of the ASME, Journal of Pressure Vessel Technology*.
28. S. Hamer et al., "Mode I and Mode II Fracture Energy of MWCNT Reinforced Nanofibrilmats Interleaved Carbon/Epoxy Laminates", *Composites Science and Technology* 90, p. 48-56 (2014).
29. E. Amit et al., "Time Reversal for Crack Identification", *Computational Mechanics* 54, p. 443-459 (2014).
30. Z. Yosibash and S. Shannon, "Computing edge stress intensity functions (ESIFs) along circular 3-D edges", *Engineering Fracture Mechanics* 117 p. 127–151 (2014).
31. S. Shannon, V. Peron and Z. Yosibash, "Singular asymptotic solution along an elliptical edge for the Laplace equation in 3-D", *Engineering Fracture Mechanics*, In press.
32. S. Shannon, V. Peron and Z. Yosibash, "The Laplace equation in 3-D domains with cracks: Dual singularities with log terms and extraction of corresponding edge flux intensity functions", *Mathematical Methods in Applied Sciences*, In press.
33. B. Mittelman and Z. Yosibash, "Asymptotic analysis of the potential energy difference because of a crack at a V-notch edge in a 3D domain", *Engineering Fracture Mechanics* 131, p. 232–256 (2014).
34. C. Ishbir, "Fracture and Fatigue Behavior of Plain Laminate Multi-Directional Woven Composites (the 0°/90° and +45°/-45° Interface)", Ph.D., Tel Aviv University (2014).
35. L. Banks-Sills, C. Ishbir, V. Fourman, L. Rogel and R. Eliasi, "Interface Fracture Toughness of a Multi-Directional Woven Composite", *International Journal of Fracture* 182, p. 187-207 (2013).
36. C. Ishbir, L. Banks-Sills, V. Fourman and R. Eliasi, "Delamination Propagation in a Multi-Directional Woven Composite DCB Specimen Subjected to Fatigue Loading", *Composites Part B* 66, p. 180-189 (2014).
37. L. Banks-Sills, C. Ishbir, V. Fourman and R. Eliasi, "Delamination Toughness and Crack Propagation Tests of DCB Specimens Composed of Woven Composites", (*keynote*) *Engineering Structural Integrity Assessment (ESIA12)*, Manchester, UK (2013).
38. L. Banks-Sills, C. Ishbir, V. Fourman and R. Eliasi, "Fatigue Delamination Propagation in a Multi-Directional Woven Composite", *International Conference on Experimental Mechanics (ICEM16)*, Cambridge, UK (2014).

39. L. Banks-Sills, "50<sup>th</sup> Anniversary Article: Review on Interface Fracture and Delamination of Composites", *Strain* 50, p. 98-110 (2014).
40. L. Banks-Sills, "Interface Fracture of Homogeneous Materials and Laminates - Theory and Experiment", (*invited*) *The Distinguished Lecture Series*, Peking University, Beijing, China (2013).
41. L. Banks-Sills, "Probabilistic Analysis for Interface Fracture and Delamination Failure of Composites", (*keynote*) *European Conference of Fracture (ECF20)*, Trondheim, Norway (2014).
42. L. Banks-Sills, "Probabilistic Analysis of Delamination Failure of a Cross-Ply Laminate", *Seventh International Conference on Fracture of Polymers, Composites and Adhesives*, Les Diablerets, Switzerland (2014).
43. Or Ben David, "PMMA Reinforced with Carbon Nanotubes - Characterization of Mechanical Properties", M.Sc., Tel Aviv University (2013).
44. Tal Simhi, "Determination of Mechanical and Fracture Properties of PMMA Reinforced with Carbon Nanotubes", M.Sc., Tel Aviv University (2014).
45. O. Ben David, L. Banks-Sills, J. Aboudi, V. Fourman, R. Eliasi, T. Simhi, A. Shlayer and O. Raz, "Evaluation of the Mechanical Properties of PMMA Reinforced with Carbon Nanotubes - Experiments and Modeling", *Experimental Mechanics* 54, p. 175-186 (2014).
46. T. Simchi, L. Banks-Sills, J. Aboudi, A. Shlayer, V. Fourman and R. Eliasi, "Comparison of the Mechanical Properties of PMMA Reinforced with CNTs Fabricated by Different Processes", 16th Composite Materials Symposium, Haifa, Israel (2013).
47. R. Haj-Ali and J. Aboudi, "A new and general formulation of the parametric HFGMC micromechanical method for two and three-dimensional multi-phase composites", *International journal of solids and structures* 50, p. 907-919 (2013).
48. A. Levi-Sasson et al., "Experimental determination of linear and nonlinear mechanical properties of laminated soft composite material system", *Composites Part B-Engineering* 57, p. 96-104 (2014).
49. M.P. Weiss, "Estimating fatigue cracks, from the onset of loading, in AISI 4340 specimens, under cyclic stress", *International Journal of Fatigue* 2, p. 91-96 (1992).
50. M. Weiss and Z. Hirshberg, "Crack Extension Under Variable Loading in the Short and the Long Crack Regime, Using a General Fatigue Diagram", *Fatigue and Fracture of Engineering Materials and Structures* 19, p. 241-249 (1996).
51. S. Peles and M. Weiss, "A Modified Two-Term Fatigue Life Prediction Model for Mean Stress in Steel", *Proceedings of the seventh International Fatigue Congress*, Beijing, p. 857-864 (1999).
52. D. Elata, R. Eshkenazy and M. Weiss, "The Mechanical Behavior of Wire Rope", *International Journal of Solids and Structures* 41, p. 1157-1172 (2004).
53. E. Lavie, M.Sc. thesis, Faculty of Mechanical Engineering, Technion (2015).
54. I. Kressel et al., "Validation of a UAV composite wing spar repair using an embedded optical fiber Rayleigh back-scattering distributed strain sensing", *Proceedings of the 28<sup>th</sup> ICAF Symposium*, 2015.